

Learning Dependence Structures for Econometric Inference

Ulrich Hounyo*

Department of Economics
University at Albany, SUNY

June 23, 2026

Abstract

We develop a framework for learning dependence structures from empirical dependence operators. Rather than treating cluster, factor, and sparse dependence as maintained assumptions, we represent them as covariance geometries in a common Hilbert space and summarize dependence through a low-dimensional dependence profile based on projection similarity scores. We establish identification under a principal-angle separation condition, prove consistency and asymptotic normality of the estimated profile, and derive finite-sample classification error bounds. We further show that when covariance-geometry tangent spaces overlap, no statistical procedure can distinguish the geometries at first order, providing a formal characterization of ambiguous dependence structures. Projection-residual diagnostics assess absolute goodness-of-fit and detect misspecified covariance dictionaries. Finally, we establish oracle adaptivity of profile-guided inference: dependence profiles can be used to select dependence-robust procedures in a data-driven manner, yielding inference that is asymptotically equivalent to an infeasible oracle that knows the dominant covariance geometry in advance.

Keywords: Dependence learning; covariance geometry; dependence diagnostics; dependence classification; factor dependence; multiway clustering.

JEL Classification: C12, C13, C14, C38.

*Department of Economics, University at Albany – State University of New York, Albany, NY 12222, USA. E-mail: khounyo@albany.edu.

1 Introduction

Robust inference under dependence is one of the central concerns of modern econometrics. Economic data frequently exhibit dependence arising from common institutional environments, aggregate shocks, social interactions, geographic proximity, production networks, financial interconnectedness, and repeated observations over time.

Prominent examples include cluster-robust inference (White, 1980; Liang and Zeger, 1986; Arellano, 1987; Cameron et al., 2011; Cameron and Miller, 2015), spatial and HAC-type dependence (Conley, 1999; Driscoll and Kraay, 1998), factor-based methods (Chamberlain and Rothschild, 1983; Bai and Ng, 2002; Bai, 2003), and network or sparse dependence models (Bickel and Levina, 2008; Cai and Liu, 2011; Auerbach, 2019; Leung, 2022). Although these approaches differ substantially in their assumptions, they share a common feature: the dependence structure is treated as known.

In practice, however, the underlying dependence architecture is rarely known. Firms may be exposed to common industry shocks, latent macroeconomic factors, and production-network spillovers. Regional economic outcomes may reflect state-level institutions, common national shocks, geographic spillovers, migration networks, and local interactions. The central challenge is often not merely robust inference under dependence but learning the dependence structure itself.

Motivating examples. Consider a panel of firms observed over time. Residual dependence may arise because firms are exposed to common industry shocks, latent aggregate factors, or production-network linkages. These mechanisms imply very different covariance geometries—cluster, factor, and sparse dependence—yet are often simultaneously plausible in practice.

As a second example, consider regional economic outcomes. Dependence may reflect state-level institutions, common national shocks, geographic spillovers, or migration networks. Standard robust inference procedures typically require the researcher to specify one of these dependence structures in advance.

In both examples, the primary challenge is not merely to conduct inference under dependence, but to learn which dependence geometry is most consistent with the observed data.

This paper develops a framework for dependence structure learning. Rather than viewing cluster, factor, and sparse dependence as competing models, we view them as distinct geometric classes of covariance operators. Cluster dependence generates approximately structured-support covariance structures. Factor dependence generates approximately low-rank covari-

ance structures. Sparse dependence generates covariance structures in which dependence is concentrated among a relatively small subset of economically meaningful interactions.

The central object of interest is not a covariance estimator. Instead, the framework starts from an empirical dependence operator constructed from the sampling design. Depending on the application, this operator may correspond to a sample covariance matrix, a long-run covariance operator, a spatial dependence operator, a network dependence operator, or another empirical measure of dependence. The objective is to learn the geometry of dependence encoded in this operator.

The paper does not seek to estimate dependence by imposing a cluster, factor, or sparse model. Rather, it assumes the existence of a population dependence operator and studies what aspects of dependence geometry can be learned from a consistent estimate of that operator.

A key distinction between the present framework and existing approaches is that the object of interest is not the dependence operator itself. Even when a researcher can consistently estimate an appropriate dependence operator, the resulting object often remains high dimensional and difficult to interpret. The goal of dependence learning is therefore to recover the geometric organization encoded in the operator. The dependence profile provides a low-dimensional summary that quantifies the extent to which the operator resembles cluster, factor, and sparse covariance geometries. In this sense, dependence structures are treated as estimands rather than maintained assumptions.

Importantly, the objective is not necessarily to recover a unique dependence structure. Different covariance geometries may overlap locally, making ambiguity an inherent feature of the problem rather than a consequence of limited sample size. Dependence learning therefore seeks both to identify dominant dependence patterns and to diagnose situations in which multiple geometries provide similarly plausible descriptions of the observed dependence operator.

An analogy may help clarify the objective. As principal component analysis uses the covariance matrix to recover a low-dimensional representation of variation, our framework uses an empirical dependence operator to recover a low-dimensional representation of dependence geometry. The operator serves as an intermediate object through which the underlying dependence structure is learned.

An important feature of the framework is that it distinguishes between relative and absolute notions of dependence fit. A large similarity score indicates that one covariance geometry provides a better approximation than the alternatives under consideration, but it does not imply that the geometry provides a good approximation in an absolute sense. To address this issue, we introduce projection-residual diagnostics that measure the distance between

the empirical dependence operator and the closest covariance geometry. These diagnostics allow the researcher to distinguish between clear geometric classifications, ambiguous dependence structures arising from overlapping covariance geometries, and situations in which none of the candidate geometries adequately captures the observed dependence pattern.

A central theme of the paper is the distinction between identifiable and ambiguous dependence structures. Identification is governed by the geometric separation of covariance classes. When covariance geometries are sufficiently separated, dependence profiles are locally identifiable and support reliable classification. When covariance geometries overlap, however, ambiguity may be intrinsic rather than a consequence of limited sample size. We show that the principal-angle condition, applied to the off-diagonal (dependence-relevant) part of each tangent space, provides a geometric identification criterion: positive principal angles ensure local distinguishability, whereas overlapping tangent spaces generate local indistinguishability. Theorem 1 characterizes the identifiable region of the covariance-geometry space, while Theorem 2 characterizes the boundary at which identification fails. Together, the two results delineate the boundary between identifiable and fundamentally ambiguous dependence structures.

The proposed dependence profile is also conceptually related to several familiar ideas in econometrics. In factor models, researchers often summarize variation through factor contribution measures. In forecast combination and model averaging, weights summarize the relative importance of competing predictive models (Bates and Granger, 1969; Hansen, 2007). In semiparametric efficiency theory, projection operators characterize efficient influence functions through orthogonal projections onto tangent spaces (Newey, 1994; Bickel et al., 1993). The dependence profile serves a similar descriptive purpose: it does not represent an additive covariance decomposition, but summarizes the relative geometric proximity of the observed dependence operator to economically meaningful dependence classes.

Existing robust inference methods require the researcher to specify a dependence structure in advance. Our framework instead quantifies the extent to which alternative covariance geometries are supported by the data. To formalize this idea, we introduce projection operators onto cluster, factor, and sparse covariance classes, which induce a dependence profile $(\omega_C, \omega_F, \omega_S)$. These classes should be viewed as illustrative benchmark geometries rather than an exhaustive collection.

A central objective of the paper is not only to learn dependence structures, but also to use this information to guide econometric inference. We show that estimated dependence profiles can be used to construct profile-guided procedures that adapt to the dominant dependence geometry. Under suitable conditions, the resulting procedures are asymptotically equivalent to an infeasible oracle that knows the dominant covariance geometry in advance.

Simulation evidence shows that profile-guided inference closely approximates the infeasible oracle procedure across a broad range of dependence environments.

The paper’s theoretical contribution is organized around three principal results. Theorem 1 establishes local identification of dependence profiles under a principal-angle separation condition. Theorem 2 shows that when covariance geometries share common tangent directions, no statistical procedure can distinguish them at first order. Finally, Theorem 7 establishes oracle adaptivity of profile-guided inference, showing that dependence learning can be used to construct inference procedures that are asymptotically equivalent to an infeasible oracle that knows the dominant covariance geometry in advance. The paper makes five contributions.

Geometric framework. We represent dependence structures as covariance geometries—closed subsets of the Hilbert space of symmetric matrices—and characterize their local structure through tangent spaces and principal angles. Cluster, factor, and sparse dependence are treated as geometric classes rather than competing maintained assumptions. The framework itself is not tied to these particular classes and can accommodate other covariance geometries, including spatial, network, long-memory, or other application-specific dependence structures.

Identification and estimation. We establish local identification of the dependence profile under a principal-angle separation condition, prove consistency, and derive asymptotic normality of the estimated dependence profile. Projection-residual diagnostics provide a complementary absolute goodness-of-fit measure.

Classification theory. We establish consistency of dominant-geometry classification (Theorem 5), derive finite-sample error bounds based on the separation margin Δ_ω (Proposition 2), and characterize classification probabilities under local near-tie alternatives (Theorem 6).

Geometric ambiguity. We show that when two covariance-geometry tangent spaces share a common direction, no sequence of tests can distinguish the geometries at first order (Theorem 2). This impossibility result explains ambiguous dependence profiles and near-ties as consequences of local nonidentification rather than finite-sample noise.

Adaptive inference. We establish oracle adaptivity of profile-guided inference (Theorem 7). Estimated dependence profiles can be used to select dependence-robust procedures in a data-driven manner, and the resulting inference is asymptotically equivalent to an infeasible oracle that knows the dominant covariance geometry in advance.

1.1 Related Literature

This paper contributes to several strands of econometrics. First, it relates to inference under dependence, including clustered dependence (Liang and Zeger, 1986; Arellano, 1987; Cameron et al., 2011), spatial dependence (Conley, 1999; Driscoll and Kraay, 1998), network dependence (Auerbach, 2019; Leung, 2022), and factor dependence (Chamberlain and Rothschild, 1983; Bai and Ng, 2002; Bai, 2003). These methods generally assume that the relevant dependence architecture is known.

Second, the paper relates to covariance regularization and high-dimensional dependence modeling. Sparse covariance estimation exploits localized dependence structures (Bickel and Levina, 2008; Cai and Liu, 2011; Friedman et al., 2008), while factor models exploit low-rank covariance representations. Our framework does not seek to select a single covariance model, but to quantify geometric proximity to multiple covariance geometries.

Third, the paper is related to low-rank plus sparse decomposition and robust principal component analysis (Candès et al., 2011; Chandrasekaran et al., 2011). Those methods aim to recover structural matrix decompositions. By contrast, our objective is to characterize the dependence architecture through similarity scores, allowing multiple mechanisms to coexist.

Finally, the paper draws on projection theory, matrix geometry, and semiparametric projection methods (Deutsch, 2001; Absil et al., 2008; Newey, 1994; Bickel et al., 1993). The principal-angle condition introduced below plays a central role in geometric identification and clarifies the sources of ambiguous dependence structures.

The paper is organized as follows. Section 2 introduces the covariance geometry framework. Section 3 develops identification and ambiguity results. Sections 4 and 5 study estimation and asymptotic theory. Section 6 develops dependence diagnostics and classification. Section 7 presents profile-guided inference. Sections 8 and 9 report simulation and empirical evidence.

2 Covariance Geometry Framework

Let

$$u = (u_1, \dots, u_n)'$$

denote the disturbance vector and define

$$\Sigma = E(uu').$$

We view Σ as an element of the Hilbert space

$$\mathbb{H} = \{A = A' : \|A\|_F < \infty\}, \quad \langle A, B \rangle_F = \text{tr}(A'B).$$

Rather than assuming that Σ belongs to a single dependence class, we characterize its dependence architecture through its geometric proximity to several economically meaningful covariance classes.

2.1 Covariance Classes

Let

$$\mathcal{S}_C, \quad \mathcal{S}_F, \quad \mathcal{S}_S$$

denote cluster, factor, and sparse covariance classes.

A covariance matrix belongs to the cluster class \mathcal{S}_C if its support can be represented as the union of a finite number of clustering dimensions. Suppose there are M clustering dimensions and let $g_m(i)$, $m = 1, \dots, M$, denote the cluster membership of observation i along dimension m . Define the *cluster-support matrix* M_C by

$$(M_C)_{ij} = \mathbf{1}\left\{g_m(i) = g_m(j) \text{ for at least one } m \in \{1, \dots, M\}\right\}.$$

Thus $(M_C)_{ij} = 1$ whenever observations i and j share at least one cluster membership, and $(M_C)_{ij} = 0$ otherwise. A covariance matrix Γ belongs to \mathcal{S}_C if $\Gamma_{ij} = 0$ whenever $(M_C)_{ij} = 0$, equivalently if $\Gamma = M_C \odot \Gamma$. This definition includes one-way clustering ($M = 1$), two-way clustering ($M = 2$), and multiway clustering ($M \geq 2$) as special cases.

For a fixed or slowly growing rank r , define the factor class as

$$\mathcal{S}_F(r) = \left\{ \Gamma \succeq 0 : \Gamma = L + D, \text{ rank}(L) \leq r, D \text{ diagonal} \right\}.$$

For $k_n = o(n^2)$, define the sparse class as

$$\mathcal{S}_S = \left\{ \Gamma \in \mathbb{H} : |\text{supp}(\Gamma)| \leq k_n \right\}.$$

The covariance dictionary considered in this paper consists of cluster, factor, and sparse geometries. These serve as benchmark geometries for illustration; the framework extends naturally to richer dictionaries.

2.2 Projection Operators

Throughout the paper, let

$$\mathfrak{D} = \{C, F, S\}$$

denote the set of covariance geometries, corresponding respectively to cluster, factor, and sparse dependence. Define

$$P_d(\Sigma) = \arg \min_{\Gamma \in \mathcal{S}_d} \|\Sigma - \Gamma\|_F.$$

$P_d(\Sigma)$ represents the closest approximation to Σ within the covariance class \mathcal{S}_d . Although we use projection notation, P_d need not be a linear orthogonal projection because the covariance classes may be nonlinear or nonconvex.

Lemma 1 (Existence of Projections). *If \mathcal{S}_d is closed in \mathbb{H} , then $P_d(\Sigma)$ exists for every $\Sigma \in \mathbb{H}$.*

Lemma 2 (Continuity of Projection Operators). *Suppose P_d is locally unique at Σ . If $\Sigma_m \rightarrow \Sigma$, then*

$$P_d(\Sigma_m) \rightarrow P_d(\Sigma).$$

2.3 Why the Frobenius Geometry?

The Frobenius norm is induced by the Hilbert inner product $\langle A, B \rangle_F = \text{tr}(A'B)$. It therefore provides a natural geometry for defining projections, tangent spaces, principal angles, and local separation between covariance classes. It is also computationally convenient: low-rank projections are based on spectral truncation, cluster projections on support masks, and sparse projections on thresholding or sparse approximation. Alternative metrics may be useful in other applications, but the Frobenius geometry gives the most transparent framework for the identification and asymptotic theory developed below.

2.4 Dependence Similarity Scores

Define

$$S_d = \|P_d(\Sigma)\|_F^2, \quad d \in \mathfrak{D}.$$

The normalized dependence similarity scores are

$$\omega_d = \frac{S_d}{\sum_{d \in \mathfrak{D}} S_d}, \quad d \in \mathfrak{D}.$$

The vector

$$\omega = (\omega_C, \omega_F, \omega_S)'$$

is called the dependence profile.

Remark 1 (No Variance Decomposition). *The quantities $\omega_C, \omega_F, \omega_S$ should not be interpreted as fractions of covariance explained. Since the covariance geometries overlap and the projections are not generally orthogonal,*

$$\sum_{d \in \mathfrak{D}} S_d \neq \|\Sigma\|_F^2$$

in general. The dependence profile measures relative geometric similarity, not additive covariance contributions.

3 Geometric Identification

The dependence profile is identified through the local geometry of the covariance classes. Identification depends on whether the cluster, factor, and sparse geometries remain sufficiently separated in a neighborhood of the population dependence operator.

For each geometry $d \in \mathfrak{D}$, let $T_d(\Sigma_d)$ denote the corresponding tangent space at a regular point Σ_d . Since diagonal perturbations are common to all covariance geometries and carry no information about cross-sectional dependence, identification is based on the off-diagonal tangent spaces

$$T_d^{\text{off}}(\Sigma_d) = \{H \in T_d(\Sigma_d) : H_{ii} = 0 \text{ for all } i\}, \quad d \in \mathfrak{D}.$$

Principal-Angle Condition. For two tangent spaces U and V , define the smallest principal angle by

$$\theta(U, V) = \inf_{u \in U, v \in V} \arccos \left(\frac{\langle u, v \rangle_F}{\|u\|_F \|v\|_F} \right).$$

Assumption 1 (Principal-Angle Identification). *There exists $\theta_0 > 0$ such that*

$$\theta(T_i^{\text{off}}(\Sigma_i), T_j^{\text{off}}(\Sigma_j)) \geq \theta_0$$

for all $i \neq j, i, j \in \mathfrak{D}$.

Formal definitions of the covariance geometries, regularity conditions, and tangent spaces are given in the Online Appendix.

Assumption 2 (Sparse Projection Regularity). *The population dependence operator Γ_0 is a regular sparse point: the k_n -th and $(k_n + 1)$ -th largest absolute off-diagonal entries of Γ_0 are distinct.*

Lemma 3 (Principal Angle and Tangent-Space Transversality). *Let U and V be closed linear subspaces of \mathbb{H} . Then $\theta(U, V) > 0$ if and only if $U \cap V = \{0\}$.*

Theorem 1 (Local Identification of the Dependence Profile). *Suppose Assumptions 1 and 2 hold. Then the dependence profile $(\omega_C, \omega_F, \omega_S)$ is locally identified.*

Moreover, no nonzero off-diagonal perturbation direction lies simultaneously in two distinct covariance geometries. Consequently, local changes in the dependence profile admit a unique first-order geometric interpretation.

Remark 2 (Interpretation). *Theorem 1 establishes that dependence geometries are locally distinguishable whenever their off-diagonal tangent spaces remain sufficiently separated. The principal-angle condition therefore plays the role of an identification assumption for dependence structure.*

Assumption 3 (Local Asymptotic Normality). *The statistical model $\{P_\Gamma : \Gamma \in \mathbb{H}\}$ satisfies local asymptotic normality (LAN) at Γ_0 : for every bounded sequence $H_n \rightarrow H$ in \mathbb{H} ,*

$$\log \frac{dP_{\Gamma_0+n^{-1/2}H_n}^n}{dP_{\Gamma_0}^n} = \frac{1}{\sqrt{n}} \sum_{i=1}^n \ell_i(H) - \frac{1}{2} \|H\|_{\mathcal{I}}^2 + o_p(1),$$

where $\ell_i(H)$ is a zero-mean score with $E[\ell_i(H)^2] = \|H\|_{\mathcal{I}}^2$ for a positive-definite inner product $\|\cdot\|_{\mathcal{I}}$ on \mathbb{H} .

Assumption 3 is standard. For Gaussian observations with covariance Γ_0 , LAN holds with the Fisher information inner product induced by the Gaussian log-likelihood; see Le Cam and Yang (2000), Chapter 7.

Theorem 2 (Two-Geometry Local Indistinguishability). *Let \mathcal{S}_i and \mathcal{S}_j be two covariance geometries with $i \neq j$. Suppose Assumption 3 holds at a regular point $\Gamma_0 \in \mathcal{S}_i \cap \mathcal{S}_j$, and that there exists a nonzero off-diagonal direction $H \in T_i^{off}(\Gamma_0) \cap T_j^{off}(\Gamma_0)$.*

Let $\Gamma_{i,n} \in \mathcal{S}_i$ and $\Gamma_{j,n} \in \mathcal{S}_j$ satisfy

$$\Gamma_{i,n} = \Gamma_0 + \frac{1}{\sqrt{n}}H + o(n^{-1/2}), \quad \Gamma_{j,n} = \Gamma_0 + \frac{1}{\sqrt{n}}H + o(n^{-1/2}).$$

Then, for any sequence of tests $\varphi_n \in [0, 1]$,

$$\limsup_{n \rightarrow \infty} |E_{\Gamma_{i,n}} \varphi_n - E_{\Gamma_{j,n}} \varphi_n| = 0.$$

Consequently, no test can have asymptotic size tending to zero and power tending to one for distinguishing \mathcal{S}_i from \mathcal{S}_j along these local sequences.

Remark 3 (Identification versus Ambiguity). *Theorems 1 and 2 characterize the boundary between identifiable and ambiguous dependence structures. Positive principal angles imply local identification, whereas overlapping tangent spaces imply local indistinguishability.*

4 Statistical Learning of Dependence Profiles

This section describes how the population dependence profile is estimated from an empirical dependence operator. Let $\widehat{\Gamma}_n$ denote an empirical dependence operator constructed from the data. The operator may be a covariance matrix, a long-run covariance operator, a spatial covariance operator, a network dependence operator, or another object summarizing the dependence features relevant for the inferential problem. Let Γ_0 denote the corresponding population dependence operator.

Assumption 4 (Consistency of the Empirical Dependence Operator). *There exists a population dependence operator $\Gamma_0 \in \mathbb{H}$ such that*

$$\|\widehat{\Gamma}_n - \Gamma_0\|_F = o_p(1).$$

Remark 4 (Dependence Operator versus Dependence Structure). *Assumption 4 does not require the dependence structure to be known. The assumption concerns the population dependence operator Γ_0 , which plays the role of an intermediate object. The estimands of interest are the dependence profile, the dominant covariance geometry, and the associated classification, all of which are functionals of Γ_0 .*

The situation is analogous to principal component analysis, where the covariance matrix is consistently estimated while the principal components themselves remain unknown.

The choice of $\widehat{\Gamma}_n$ is application-specific. It may be a covariance, long-run covariance, spatial, network, or cluster-supported operator. The theory below is conditional on the chosen operator; a fuller discussion of operator choice and computational implementation is given in the Online Appendix.

4.1 Choice of Dependence Operator

The empirical dependence operator should capture the form of dependence relevant for the inferential problem. For contemporaneous cross-sectional dependence, a natural benchmark is the residual covariance operator

$$\widehat{\Gamma}_n = \frac{1}{T} \sum_{t=1}^T \widehat{u}_t \widehat{u}_t', \quad \widehat{u}_t = (\widehat{u}_{1t}, \dots, \widehat{u}_{nt})'.$$

For serially dependent data one may instead use a long-run covariance operator. For spatial, network, or clustered data, the operator may incorporate distances, adjacency relations, or cluster-support restrictions.

The framework does not seek to select a unique dependence operator. Rather, it studies the covariance geometry encoded in a chosen population operator. The dependence profile is invariant to positive rescalings of the operator; additional examples and technical details are provided in the Online Appendix.

4.2 Projection Residual Diagnostics

The dependence profile provides a relative measure of geometric fit. To assess goodness-of-fit in an absolute sense, we introduce projection-residual diagnostics.

To quantify absolute goodness-of-fit, define the normalized projection residual

$$\rho_d(\Gamma) = \frac{\|\Gamma - P_d(\Gamma)\|_F}{\|\Gamma\|_F}, \quad d \in \mathfrak{D}.$$

The quantity $\rho_d(\Gamma)$ measures the fraction of the operator that remains unexplained after projection onto geometry d . Since $0 \in \mathcal{S}_d$, the definition of the projection implies

$$\|\Gamma - P_d(\Gamma)\|_F \leq \|\Gamma\|_F.$$

Consequently,

$$0 \leq \rho_d(\Gamma) \leq 1.$$

Small values indicate that geometry d provides a good approximation to the dependence operator, whereas large values indicate substantial lack of fit.

Define the minimum residual

$$\rho_{\min}(\Gamma) = \min_{d \in \mathfrak{D}} \rho_d(\Gamma).$$

The quantity $\rho_{\min}(\Gamma)$ summarizes the distance from the dependence operator to the closest covariance geometry in the dictionary.

We say that a dependence operator exhibits a “none-of-the-above” pattern whenever

$$\rho_{\min}(\Gamma) > \delta,$$

for a prespecified threshold $\delta \in (0, 1)$.

Large values of $\rho_{\min}(\Gamma)$ indicate that none of the cluster, factor, or sparse geometries pro-

vides an adequate approximation to the observed dependence structure. In such situations, the dependence profile should be interpreted with caution, since the operator may contain dependence features not represented in the covariance dictionary.

Proposition 1. *Suppose Assumption 4 hlds. Then*

$$\rho_d(\widehat{\Gamma}_n) \xrightarrow{p} \rho_d(\Gamma_0), \quad d \in \mathfrak{D},$$

and

$$\rho_{\min}(\widehat{\Gamma}_n) \xrightarrow{p} \rho_{\min}(\Gamma_0).$$

4.3 Population Dependence Profile

The population dependence profile is defined from projections of Γ_0 onto the covariance geometries. For each $d \in \mathfrak{D}$, define

$$P_{d,0} = P_d(\Gamma_0), \quad S_{d,0} = \|P_{d,0}\|_F^2.$$

The population similarity score associated with geometry d is

$$\omega_{d,0} = \frac{S_{d,0}}{\sum_{d \in \mathfrak{D}} S_{d,0}}, \quad d \in \mathfrak{D}.$$

The vector

$$\omega_0 = (\omega_{C,0}, \omega_{F,0}, \omega_{S,0})'$$

is the population dependence profile.

4.4 Similarity-Score Estimation

Define

$$\widehat{S}_d = \|\widehat{P}_d\|_F^2, \quad d \in \mathfrak{D}.$$

The estimated similarity score for geometry d is

$$\widehat{\omega}_d = \frac{\widehat{S}_d}{\sum_{d \in \mathfrak{D}} \widehat{S}_d}, \quad d \in \mathfrak{D}.$$

The estimated dependence profile is

$$\widehat{\omega} = (\widehat{\omega}_C, \widehat{\omega}_F, \widehat{\omega}_S)'$$

5 Asymptotic Theory

This section establishes consistency and asymptotic normality of the estimated dependence profile.

Assumption 5 (Asymptotic Linearity of the Dependence Operator). *There exists a mean-zero random vector ψ_i such that*

$$\sqrt{n} \operatorname{vec}(\widehat{\Gamma}_n - \Gamma_0) = \frac{1}{\sqrt{n}} \sum_{i=1}^n \psi_i + o_p(1),$$

and

$$E(\psi_i \psi_i') = \Omega_\Gamma.$$

Lemma 4 (Uniform Consistency of Projection Estimators). *Suppose Assumptions 1, 2, and 4 hold. Then*

$$\max_{d \in \mathcal{D}} \|\widehat{P}_d - P_{d,0}\|_F = o_p(1).$$

Theorem 3 (Consistency of the Dependence Profile). *Suppose Assumptions 1, 2, 4 hold. If $\sum_{d \in \mathcal{D}} S_{d,0} > 0$, then*

$$\widehat{\omega} - \omega_0 = o_p(1).$$

To state the limiting distribution, define the score map

$$\mathcal{S}(\Gamma) = (\|P_C(\Gamma)\|_F^2, \|P_F(\Gamma)\|_F^2, \|P_S(\Gamma)\|_F^2)'$$

Let

$$s_0 = \mathcal{S}(\Gamma_0) = (S_{C,0}, S_{F,0}, S_{S,0})'$$

Let

$$\pi(s) = \frac{s}{\mathbf{1}'s}$$

denote the normalization map from similarity scores to the dependence profile, where $\mathbf{1} = (1, 1, 1)'$. Thus, $\omega_0 = \pi(s_0)$.

Corollary 1 (Differentiability of the Score Map). *Suppose Assumptions 1 and 2 hold at Γ_0 . Then the score map $\mathcal{S}(\cdot)$ is Hadamard differentiable at Γ_0 , with derivative $\dot{\mathcal{S}}_{\Gamma_0}$ given coordinatewise by*

$$\dot{\mathcal{S}}_{d,\Gamma_0}[H] = 2 \langle P_d(\Gamma_0), \Pi_{T_d(\Gamma_0)}(H) \rangle_F, \quad d \in \mathfrak{D}.$$

Theorem 4 (Asymptotic Distribution of the Dependence Profile). *Suppose Assumptions 1, 2, and 5 hold. (By Corollary 1, the score map $\mathcal{S}(\cdot)$ is then automatically Hadamard differentiable at Γ_0 , with derivative $\dot{\mathcal{S}}_{\Gamma_0}$.) If $\sum_{d \in \mathfrak{D}} S_{d,0} > 0$, then*

$$\sqrt{n}(\hat{\omega} - \omega_0) \Rightarrow N(0, \Xi),$$

where $\Xi = J_\omega \Omega_\Gamma J'_\omega$, with $J_\omega = \dot{\pi}_{s_0} \dot{\mathcal{S}}_{\Gamma_0}$.

Here $\dot{\pi}_{s_0}$ is the derivative of the normalization map $\pi(s) = s/(\mathbf{1}'s)$ evaluated at s_0 .

6 Dependence Diagnostics and Classification

The dependence profile provides a low-dimensional summary of the dependence architecture encoded in the empirical dependence operator. Large values of $\hat{\omega}_C$, $\hat{\omega}_F$, and $\hat{\omega}_S$ indicate that the empirical dependence operator is geometrically close to the cluster, factor, and sparse covariance classes, respectively.

The dependence profile measures relative geometric similarity rather than additive covariance contributions. A natural classification rule is

$$\hat{d} = \arg \max_{d \in \mathfrak{D}} \hat{\omega}_d. \tag{1}$$

The estimated geometry \hat{d} identifies the covariance class with the largest estimated similarity score. The full dependence profile is often more informative than the classification alone. For example,

$$(0.60, 0.30, 0.10)$$

suggests cluster dominance with meaningful factor dependence, whereas

$$(0.35, 0.35, 0.30)$$

suggests hybrid dependence and cautions against a purely binary classification.

6.1 Statistical Uncertainty for Dependence Scores

Inference for the dependence profile is based on Theorem 4,

$$\sqrt{n}(\hat{\omega} - \omega_0) \Rightarrow N(0, \Xi),$$

where

$$\omega_0 = (\omega_{C,0}, \omega_{F,0}, \omega_{S,0})'.$$

Let

$$e_C = (1, 0, 0)', \quad e_F = (0, 1, 0)', \quad e_S = (0, 0, 1)'.$$

For $d \in \mathfrak{D}$, the asymptotic variance of $\hat{\omega}_d$ is

$$\sigma_d^2 = e_d' \Xi e_d.$$

Assumption 6 (Consistent Covariance Estimation). *There exists an estimator $\hat{\Xi}$ such that*

$$\hat{\Xi} - \Xi = o_p(1).$$

Under Assumption 6,

$$\hat{\sigma}_d^2 = e_d' \hat{\Xi} e_d$$

is a consistent estimator of σ_d^2 .

The construction of $\hat{\Xi}$ depends on the chosen empirical dependence operator. When the operator admits an asymptotic linear representation, a plug-in estimator based on the influence function and the delta method may be used. The construction of a universal variance estimator for all possible dependence operators is outside the scope of the paper.

6.2 Diagnostic Tests

To test

$$H_0 : \omega_C = \omega_C^*,$$

consider

$$T_C = \frac{\sqrt{n}(\hat{\omega}_C - \omega_C^*)}{\hat{\sigma}_C},$$

where

$$\hat{\sigma}_C^2 = e_C' \hat{\Xi} e_C.$$

Under H_0 ,

$$T_C \Rightarrow N(0, 1).$$

Analogous statistics apply to the factor and sparse scores.

More generally, let R_ω be a $q \times 3$ matrix of full row rank and consider

$$H_0 : R_\omega \omega_0 = r_\omega.$$

Define

$$W_\omega = n (R_\omega \hat{\omega} - r_\omega)' \left(R_\omega \hat{\Xi} R_\omega' \right)^{-1} (R_\omega \hat{\omega} - r_\omega).$$

Under H_0 ,

$$W_\omega \Rightarrow \chi_q^2.$$

These tests quantify the uncertainty associated with the estimated dependence profile and should be interpreted as diagnostic tools.

6.3 Dominant and Hybrid Dependence

A dominant dependence geometry is suggested when one similarity score substantially exceeds the others. For example,

$$\hat{\omega}_C > \max \{ \hat{\omega}_F, \hat{\omega}_S \}$$

indicates that the empirical dependence operator is closest to the cluster covariance geometry.

Hybrid dependence is suggested when several scores are simultaneously large. In such cases, the full dependence profile should be reported rather than reducing the analysis to a single classification label.

This distinction is important because covariance geometries may overlap. For example, cluster covariance matrices may also be sparse when cluster sizes are small relative to the sample size. The dependence profile should therefore be viewed as a continuous description of dependence architecture rather than a rigid model-selection device.

6.4 Dominant Dependence Geometry

A central question is whether the estimated dependence profile can be used to identify the dominant covariance geometry underlying the chosen dependence operator.

Assumption 7 (Unique Dominant Geometry). *There exists a unique geometry $d^* \in \mathcal{D}$ such that*

$$\omega_{d^*} > \max_{d \neq d^*} \omega_d.$$

Equivalently, the separation margin

$$\Delta_\omega = \omega_{d^*} - \max_{d \neq d^*} \omega_d$$

satisfies $\Delta_\omega > 0$.

Under Assumption 7, define

$$d^* = \arg \max_{d \in \mathfrak{D}} \omega_d. \quad (2)$$

The quantity d^* represents the population dominant dependence geometry.

Assumption 7 rules out knife-edge cases in which two or more covariance geometries have exactly the same population similarity score. Similar separation conditions are common in model selection and statistical classification problems.

Proposition 2 (Classification Error Bound). *Suppose Assumption 7 holds. Then*

$$P(\hat{d} \neq d^*) \leq P\left(\max_{d \in \mathfrak{D}} |\hat{\omega}_d - \omega_d| > \frac{\Delta_\omega}{2}\right),$$

where

$$\Delta_\omega = \omega_{d^*} - \max_{d \neq d^*} \omega_d.$$

Theorem 5 (Consistency of Dominant-Geometry Classification). *Suppose the conditions of Theorem 3 hold so that*

$$\hat{\omega}_d \xrightarrow{p} \omega_d, \quad d \in \mathfrak{D},$$

and Assumption 7 holds. Then

$$P(\hat{d} = d^*) \longrightarrow 1.$$

Theorem 5 shows that the dependence profile consistently identifies the dominant covariance geometry whenever the dominant similarity score is separated from the remaining scores. Consequently, the dependence profile is not merely a descriptive summary of dependence but also provides a statistically consistent basis for dependence classification.

Remark 5 (Relation to Statistical Classification). *Theorem 5 is analogous to consistency results in model selection and statistical classification. The distinguishing feature here is that the objects being classified are covariance geometries rather than parametric models.*

The classification result provides a formal justification for using the estimated dependence profile as a guide for procedure recommendation. The implications for inference are developed formally in Section 7.

Theorem 6 (Local Alternatives and Near-Ties). *Suppose*

$$\sqrt{n}(\widehat{\omega} - \omega_n) \Rightarrow N(0, \Xi),$$

where

$$\omega_n = (\omega_{C,n}, \omega_{F,n}, \omega_{S,n})'.$$

Assume that two geometries, d_1 and d_2 , satisfy

$$\omega_{d_1,n} - \omega_{d_2,n} = \frac{c}{\sqrt{n}},$$

for some constant $c \in \mathbb{R}$, while all remaining scores remain separated by positive constants.

Then

$$P(\widehat{d} = d_1)$$

converges to a nondegenerate limit lying strictly between zero and one.

Remark 6 (Near-Ties). *When the separation margin Δ_ω is close to zero, small sampling fluctuations may alter the dominant geometry classification. In such situations, the full dependence profile $\widehat{\omega} = (\widehat{\omega}_C, \widehat{\omega}_F, \widehat{\omega}_S)'$ is typically more informative than the discrete classifier \widehat{d} .*

7 Profile-Guided Inference

The dependence profile provides a low-dimensional summary of the dependence geometry encoded in an empirical dependence operator. A natural question is whether the estimated profile can be used to guide econometric inference. The objective of this section is not to propose a new covariance estimator. Rather, we show how dependence learning can be combined with existing dependence-robust procedures in a systematic way.

7.1 Profile-Guided Procedure Recommendation

Let \hat{d} denote the estimated dominant dependence geometry as defined in (1). The interpretation is straightforward. When $\hat{\omega}_C$ dominates, cluster-robust procedures provide a natural benchmark. When $\hat{\omega}_F$ dominates, factor-robust or common-shock-adjusted procedures are suggested. When $\hat{\omega}_S$ dominates, sparse, network, spatial, or local-dependence robust procedures deserve particular attention.

The recommendation should be viewed as evidence-based rather than deterministic. The dependence profile does not imply that one procedure is universally correct. Rather, it summarizes which covariance geometry appears most consistent with the observed dependence operator.

When multiple similarity scores are substantial, the data provide evidence for several dependence mechanisms simultaneously. In such situations, reporting inference results from multiple dependence-robust procedures may be preferable. Similarly, when the projection-residual diagnostics indicate poor fit, the entire covariance dictionary should be viewed with caution.

7.2 Why Learn the Geometry?

A natural alternative is to use a single broadly robust procedure, such as multiway clustering, HAC inference, or a general sandwich estimator. Dependence learning remains useful for three reasons.

First, broad robustness is not costless. Procedures designed to be valid under large classes of dependence may be conservative or poorly sized when the realized dependence geometry differs from the structure for which the procedure is best suited. Second, such procedures still require the researcher to specify a dependence class, such as clustering dimensions, a spatial metric, a bandwidth, or a network. These choices are themselves assumptions about dependence. Third, Theorem 7 shows that profile-guided selection is asymptotically equivalent to an infeasible oracle that knows the dominant covariance geometry.

Thus, the value of dependence learning is not only diagnostic. It provides a data-driven way to choose among geometry-specific inference procedures while retaining oracle-equivalent first-order behavior.

7.3 Procedure Confidence Index

The reliability of a profile-based procedure recommendation depends on two considerations. First, the dominant geometry should be sufficiently separated from the competing geometries.

Define the estimated separation margin

$$\widehat{\Delta}_\omega = \max_{d \in \mathfrak{D}} \widehat{\omega}_d - \max_{d \neq \widehat{d}} \widehat{\omega}_d.$$

Second, the covariance dictionary should provide a satisfactory approximation to the empirical dependence operator. Recall the minimum projection residual

$$\widehat{\rho}_{\min} = \min_{d \in \mathfrak{D}} \widehat{\rho}_d.$$

Combining these quantities yields the procedure confidence index

$$\widehat{\kappa} = (1 - \widehat{\rho}_{\min}) \widehat{\Delta}_\omega.$$

Large values of $\widehat{\kappa}$ indicate that one geometry is clearly dominant and that the covariance dictionary provides a good approximation to the observed dependence operator. Small values indicate either weak separation, poor geometric fit, or both.

The index therefore summarizes the strength of the empirical evidence supporting a profile-based procedure recommendation. Let

$$\kappa_0 = (1 - \rho_{\min,0}) \Delta_{\omega,0}, \quad \rho_{\min,0} = \min_{d \in \mathfrak{D}} \rho_d, \quad \Delta_{\omega,0} = \max_{d \in \mathfrak{D}} \omega_d - \max_{d \neq d^*} \omega_d, \quad \text{with } d^* = \arg \max_{d \in \mathfrak{D}} \omega_d.$$

Proposition 3 (Consistency of the Procedure Confidence Index). *Suppose the conditions of Theorem 3 hold. Then*

$$\widehat{\kappa} \xrightarrow{p} \kappa_0.$$

7.4 Profile-Guided Variance Estimation

Suppose a scalar parameter θ_0 is estimated by $\widehat{\theta}_n$. For each geometry $d \in \mathfrak{D}$, let \widehat{V}_d be a measurable variance estimator and let $\tau_{n,d} \rightarrow \infty$ be a deterministic normalization such that

$$\tau_{n,d}^2 \text{Var}(\widehat{\theta}_n) \longrightarrow V_d, \quad 0 < V_d < \infty.$$

Define

$$\widehat{d} = \arg \max_{d \in \mathfrak{D}} \widehat{\omega}_d, \quad \widehat{V}^* = \widehat{V}_{\widehat{d}},$$

where ties in the argmax are broken by a fixed deterministic rule. Thus, inference is based on the variance estimator associated with the estimated dominant dependence geometry.

Proposition 4 (Consistency of the Profile-Guided Variance Estimator). *Let \widehat{V}_d denote a geometry-specific variance estimator for $d \in \mathfrak{D}$. Suppose the conditions of Theorem 5 hold and*

$$\widehat{V}_{d^*} \xrightarrow{p} V_{d^*},$$

where

$$d^* = \arg \max_{d \in \mathfrak{D}} \omega_d.$$

Then

$$\widehat{V}^* \xrightarrow{p} V_{d^*}.$$

Proposition 4 shows that profile-guided selection preserves consistency whenever the dominant geometry is correctly classified. The next result establishes a stronger oracle property.

Theorem 7 (Oracle adaptivity of profile-guided inference). *Suppose the conditions of Theorem 5 hold. Let $d^* = \arg \max_{d \in \mathfrak{D}} \omega_d$ denote the dominant covariance geometry, and let \widehat{V}_d be a variance estimator satisfying*

$$\widehat{V}_d \xrightarrow{p} V_d, \quad d \in \mathfrak{D}.$$

Define

$$\widehat{d} = \arg \max_{d \in \mathfrak{D}} \widehat{\omega}_d, \quad \widehat{V}^* = \widehat{V}_{\widehat{d}}.$$

Then

$$\widehat{V}^* - \widehat{V}_{d^*} = o_p(1).$$

Consequently,

$$\widehat{V}^* \xrightarrow{p} V_{d^*}.$$

Thus, the profile-guided variance estimator is asymptotically equivalent to the infeasible oracle estimator that knows the dominant covariance geometry in advance.

When the asymptotic normalization depends on the covariance geometry, comparison with the oracle statistic is naturally made on the event $\{\widehat{d} = d^*\}$. On this event the selected rate $\tau_{n,\widehat{d}}$ and variance estimator \widehat{V}^* coincide exactly with τ_{n,d^*} and \widehat{V}_{d^*} . Since this event occurs

with probability approaching one, the profile-guided and oracle statistics are asymptotically equivalent.

Corollary 2 (Oracle-equivalent Wald inference). *Let*

$$T_n^* = \frac{\tau_{n,\hat{d}}(\hat{\theta}_n - \theta_0)}{\sqrt{\hat{V}^*}}$$

and

$$T_n^{oracle} = \frac{\tau_{n,d^*}(\hat{\theta}_n - \theta_0)}{\sqrt{\hat{V}_{d^*}}}.$$

Assume furthermore that the oracle statistic satisfies

$$T_n^{oracle} \Rightarrow N(0, 1).$$

Under the assumptions of Theorem 7,

$$T_n^* - T_n^{oracle} = o_p(1).$$

Consequently,

$$T_n^* \Rightarrow N(0, 1)$$

whenever the oracle statistic is asymptotically standard normal.

Theorem 7 and Corollary 2 provide the main econometric payoff of dependence learning. Estimated profiles can be used to select dependence-robust procedures in a data-driven way, and the resulting inference is asymptotically equivalent to the infeasible oracle procedure that knows the dominant dependence geometry in advance.

7.5 Profile-Weighted Inference

The profile-guided estimator selects a single dominant geometry. An alternative approach is to combine multiple procedures using the estimated dependence profile itself. Define

$$\hat{V}^{\text{avg}} = \sum_{d \in \mathfrak{D}} \hat{\omega}_d \hat{V}_d.$$

The resulting estimator may be interpreted as a dependence-weighted combination of geometry-specific variance estimators, analogous to forecast combination and model aver-

aging (Bates and Granger, 1969; Hansen, 2007). Developing efficiency theory and optimal weighting schemes for profile-weighted inference is an important direction for future research.

8 Simulation Evidence

This section summarizes Monte Carlo evidence for the dependence-learning framework. The simulations focus on three questions. First, can the estimated dependence profile recover the dominant covariance geometry? Second, how does classification behave under hybrid and near-tie dependence? Third, does profile-guided inference behave like the infeasible oracle procedure that knows the dominant dependence geometry in advance?

The detailed data-generating processes, parameter calibrations, projection algorithms, and additional robustness exercises are reported in the Online Appendix. The baseline designs include pure cluster, pure factor, sparse network, cluster-factor hybrid, cluster-sparse hybrid, factor-sparse hybrid, all-three hybrid, and two-way cluster dependence.

8.1 Dependence Learning

Table 1 reports the population dependence profiles and the Monte Carlo behavior of the estimated profiles. The profile recovers the dominant geometry in the benchmark cluster and factor designs and records substantial sparse affinity under designs in which support restrictions are important, including two-way clustering. The procedure confidence index κ_0 is largest when one geometry is clearly separated and the covariance dictionary provides a good absolute fit.

Table 1: Estimated Dependence Profiles

Design	ω_C	ω_F	ω_S	κ_0	MC $\widehat{\omega}_C$	MC $\widehat{\omega}_F$	MC $\widehat{\omega}_S$	SD $\widehat{\omega}_C$	SD $\widehat{\omega}_F$	SD $\widehat{\omega}_S$	RMSE
Cluster	0.555	0.101	0.345	0.210	0.454	0.200	0.346	0.009	0.015	0.008	0.142
Factor	0.039	0.705	0.257	0.448	0.039	0.706	0.255	0.001	0.004	0.004	0.006
Sparse	0.332	0.332	0.336	0.004	0.278	0.313	0.409	0.002	0.004	0.002	0.093
Cluster-Factor	0.067	0.678	0.255	0.348	0.067	0.679	0.254	0.011	0.012	0.005	0.017
Cluster-Sparse	0.549	0.107	0.344	0.203	0.449	0.205	0.346	0.008	0.013	0.007	0.141
Factor-Sparse	0.039	0.704	0.257	0.446	0.039	0.706	0.255	0.001	0.004	0.004	0.006
All Three	0.068	0.677	0.255	0.347	0.068	0.677	0.254	0.011	0.012	0.006	0.017
Two-way Cluster	0.661	0.164	0.175	0.486	0.521	0.248	0.231	0.013	0.017	0.006	0.175

Notes: The table reports population similarity scores, Monte Carlo means and standard deviations of the estimated scores, the root mean squared error of the estimated profile, and the population procedure confidence index κ_0 . Similarity scores measure relative geometric proximity and should not be interpreted as additive variance shares.

Figure 1 shows the average estimated profile along a cluster-factor hybrid path. The profile changes smoothly as the relative strength of factor dependence increases, illustrating

that the method summarizes hybrid dependence rather than forcing a binary classification.

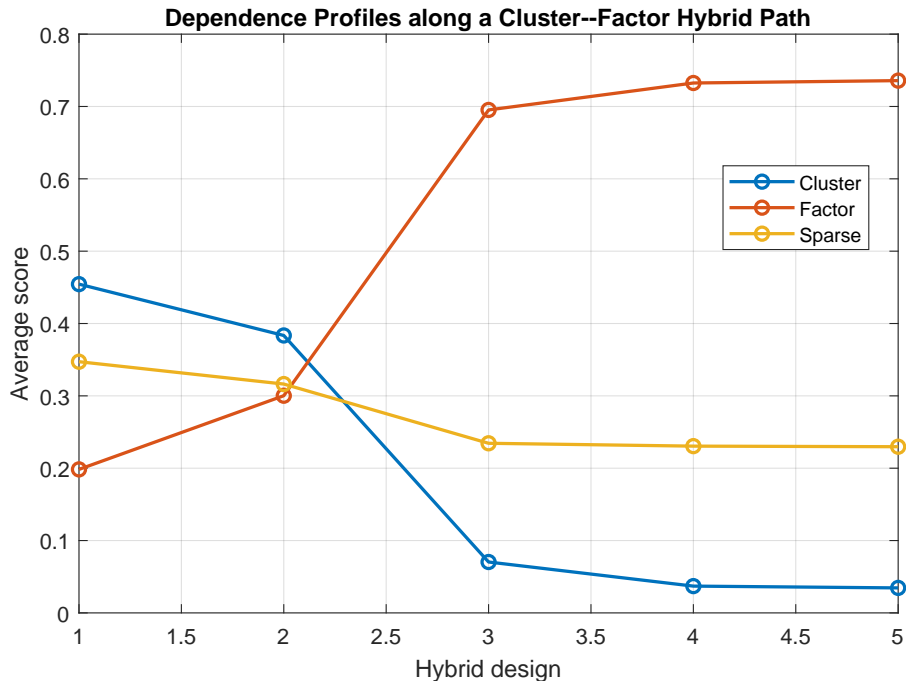


Figure 1: Dependence Profiles along a Cluster-Factor Hybrid Path
Notes: The figure plots average estimated similarity scores along a path moving from cluster-dominant to factor-dominant dependence.

8.2 Classification and Ambiguity

The classification theory predicts that dominant-geometry classification is reliable when the separation margin is large and remains probabilistic under local near-ties. Table 2 reports classification frequencies for local cluster-factor alternatives, and Figure 2 plots the relationship between classification error and the population separation margin.

8.3 Oracle-Equivalent Inference

The main econometric implication of Section 7 is that profile-guided inference should be asymptotically equivalent to an infeasible oracle procedure. Table 3 reports finite-sample coverage probabilities for the oracle procedure, the profile-guided procedure, and a deliberately misspecified procedure.

The profile-guided procedure is nearly indistinguishable from the oracle procedure across the benchmark designs, while the misspecified procedure can exhibit severe undercoverage. These results provide finite-sample support for Theorem 7 and Corollary 2. They also give

Table 2: Near-Ties and Ambiguous Dependence

c	$P_B(\hat{d} = C)$	$P_B(\hat{d} = F)$	$P_B(\hat{d} = S)$	Δ_ω
-4.0	0.000	1.000	0.000	0.435
-2.0	0.000	1.000	0.000	0.375
-1.0	0.000	1.000	0.000	0.282
0.0	0.155	0.845	0.000	0.017
1.0	0.917	0.083	0.000	0.144
2.0	1.000	0.000	0.000	0.180
4.0	1.000	0.000	0.000	0.213

Notes: The table reports Monte Carlo classification frequencies under local cluster-factor alternatives. Near-ties generate nondegenerate classification probabilities, as predicted by the local alternatives theory.

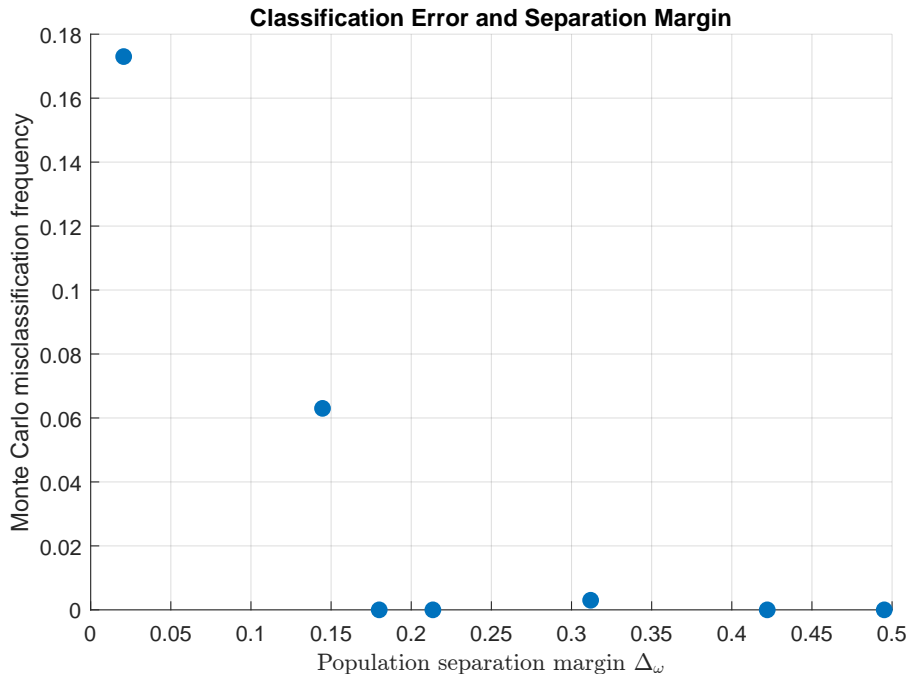


Figure 2: Classification Error and Separation Margin

Notes: The figure plots Monte Carlo misclassification frequency against the population separation margin. Larger margins are associated with lower classification error.

the main practical message of the paper: learning the dependence profile can guide the choice of robust inference procedure in a way that tracks the infeasible oracle benchmark.

9 Empirical Illustration

This section illustrates how the proposed dependence profile and projection-residual diagnostics can be used in an empirical setting. The goal is not to provide a new asset-pricing

Table 3: Oracle Equivalence of Profile-Guided Inference

DGP	Oracle Coverage	Profile-Guided Coverage	Wrong Procedure
Cluster	92.8	92.8	24.0
Factor	94.2	94.2	21.5
Sparse	95.0	95.0	25.1

Notes: The table reports empirical coverage probabilities for nominal 95% confidence intervals. The oracle procedure uses the variance estimator associated with the true dominant covariance geometry. The profile-guided procedure uses the estimated dominant geometry. The “Wrong Procedure” column reports a deliberately misspecified benchmark.

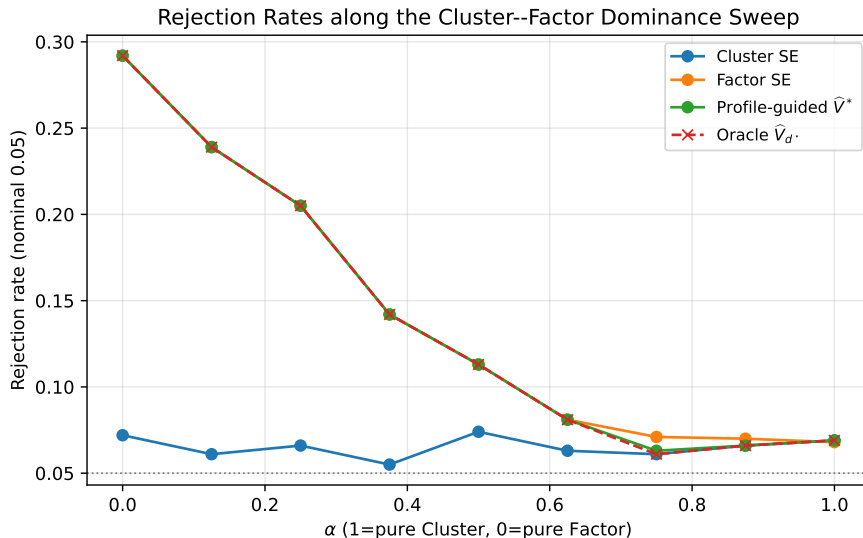


Figure 3: Oracle Tracking along a Cluster–Factor Dominance Sweep

Notes: The figure compares rejection rates for fixed procedures, the profile-guided procedure, and the infeasible oracle along a cluster–factor dominance sweep. The profile-guided and oracle procedures closely coincide when classification is reliable.

analysis, but to show how the framework can be applied to a publicly available dataset in which several dependence mechanisms are plausible.

We use the Fama–French 49 industry portfolios and the Fama–French three factors from the data library of Fama and French (1993) and French (2025). The data contain value-weighted and equal-weighted returns for U.S. industry portfolios and are available at daily, monthly, and annual frequencies. The monthly and daily series begin in July 1926. The Data Library also provides the standard asset-pricing factors used in empirical finance.

The empirical setting is well suited to the proposed framework. Industry portfolio returns may exhibit cluster-like dependence because industries can be grouped into broader sectors. They may exhibit factor dependence because returns load on common market-wide and macro-financial shocks. They may also exhibit sparse dependence because some indus-

tries are more closely linked through input-output relationships, supply chains, or common demand shocks than others.

9.1 Data and Regression Specification

The empirical analysis uses monthly excess returns on the 49 industry portfolios together with the market, SMB, and HML factors from the Kenneth R. French Data Library (French, 2025). Let R_{it} denote the excess return on industry portfolio i in month t , where $i = 1, \dots, N$, and $t = 1, \dots, T$. In the baseline illustration, $N = 49$. We estimate the factor model

$$R_{it} = \alpha_i + \beta_{iM}MKT_t + \beta_{iS}SMB_t + \beta_{iH}HML_t + u_{it}, \quad (3)$$

where MKT_t , SMB_t , and HML_t denote the Fama–French market, size, and value factors. The residual u_{it} captures the component of industry returns not explained by the observed factors.

Stack residuals across industries as $\hat{u}_t = (\hat{u}_{1t}, \dots, \hat{u}_{Nt})'$.

The baseline empirical dependence operator is the residual covariance matrix

$$\hat{\Gamma} = \frac{1}{T} \sum_{t=1}^T \hat{u}_t \hat{u}_t'. \quad (4)$$

We also consider the residual correlation operator

$$\hat{\Gamma}^{COR} = \hat{D}^{-1/2} \hat{\Gamma} \hat{D}^{-1/2}, \quad (5)$$

where $\hat{D} = \text{diag}(\hat{\Gamma})$. The covariance operator preserves differences in residual volatility across industries, whereas the correlation operator focuses on dependence geometry after normalizing scale.

9.2 Dependence Classes and Projections

We compute projections of the empirical dependence operator onto the cluster, factor, and sparse covariance geometries.

Cluster Geometry. The cluster geometry introduced in this paper encompasses one-way, two-way, and multiway clustering through a structured-support representation. In the present empirical application, we use a one-way clustering specification based on the Fama–French 10-sector economic classification (Consumer Non-Durables, Consumer Durables, Manufacturing, Energy, Hi-Tech, Telecom, Shops, Health, Utilities, and Other).

Let

$$g(i) \in \{1, \dots, G\}$$

denote the sector membership of industry portfolio i . Define the cluster-support matrix

$$(M_C)_{ij} = \mathbf{1}\{g(i) = g(j)\}.$$

The cluster projection is

$$\hat{P}_C = M_C \odot \hat{\Gamma}.$$

Thus, the empirical implementation treats industry sectors as the relevant clustering dimension and measures the extent to which the residual dependence operator conforms to the resulting cluster-support structure. If additional clustering dimensions were available, the cluster-support matrix could be constructed according to the multiway definition in Section 2.

Factor Geometry. The factor projection \hat{P}_F is computed by the alternating-projection algorithm described in Online Appendix, applied to the empirical dependence operator $\hat{\Gamma}$. The output decomposes as $\hat{P}_F = L^* + D^*$, where L^* is a rank- r positive-semidefinite matrix and D^* is diagonal. In the baseline implementation, r is selected using an eigenvalue-ratio criterion applied to $\hat{\Gamma} - \hat{D}$, where \hat{D} is the diagonal of $\hat{\Gamma}$. As robustness checks, we also consider fixed ranks $r \in \{1, 2, 3\}$.

Sparse Geometry. The sparse projection is computed by retaining the k_N largest off-diagonal entries of $\hat{\Gamma}$ in absolute value and setting all remaining off-diagonal entries to zero. The diagonal entries are retained. Formally,

$$\hat{P}_S = \arg \min_{\Gamma \in \mathcal{S}_S} \|\hat{\Gamma} - \Gamma\|_F^2.$$

This projection provides the closest sparse approximation to the empirical dependence operator under Frobenius loss.

9.3 Estimated Dependence Profiles and Residual Diagnostics

We apply the estimated dependence profile and projection-residual diagnostics defined in Sections 4.4 and 4.2, with $\hat{\Gamma}$ taken to be the residual covariance operator in (4).

The dependence profile and the projection residuals answer different questions. The

profile describes which geometry provides the strongest relative fit among the candidate classes. The residual diagnostics assess absolute fit. A large value of $\widehat{\rho}_{\min}$ indicates that none of the candidate geometries provides a close approximation to the empirical dependence operator, even if one geometry receives the largest relative similarity score.

A large $\widehat{\omega}_C$ indicates that residual dependence is well described, in relative terms, by a cluster-support structure. In the present application this corresponds to dependence concentrated within broad industry sectors. A large $\widehat{\omega}_F$ suggests that the residual covariance still contains low-rank common components not fully absorbed by the observed Fama–French factors. A large $\widehat{\omega}_S$ indicates that dependence is concentrated among a relatively small subset of industry pairs.

9.4 Conventional Robust Inference Benchmarks

To connect the dependence profile with conventional robust inference, we compare standard errors for a pooled regression of industry excess returns on the Fama–French factors. Specifically, estimate

$$R_{it} = \alpha + \beta_M MKT_t + \beta_S SMB_t + \beta_H HML_t + e_{it}. \quad (6)$$

We report heteroskedasticity-robust standard errors, standard errors clustered by broad industry sector, and two-way clustered standard errors by industry and month. We also report a common-shock benchmark that removes leading principal components from the residual covariance operator before computing standard errors.

The purpose of this comparison is descriptive. If the estimated profile assigns substantial weight to the cluster geometry, clustered standard errors should be viewed as empirically relevant. If the factor score is large, then procedures that account for common shocks or factor dependence deserve attention. If the sparse score is large, then network- or sparse-dependence robust procedures may be important. The dependence profile therefore serves as a diagnostic summary of the covariance architecture underlying the robust inference procedures considered in practice.

9.5 Empirical Results

Table 4 reports the estimated dependence profiles and projection-residual diagnostics for the residual covariance and correlation operators.

Figure 4 displays the estimated dependence profiles graphically.

Table 5 compares conventional robust standard errors for the pooled factor regression.

Table 4: Dependence Profiles and Projection-Residual Diagnostics for Industry Portfolio Residuals

Operator	$\hat{\omega}_C$	$\hat{\omega}_F$	$\hat{\omega}_S$	$\hat{\rho}_C$	$\hat{\rho}_F$	$\hat{\rho}_S$	$\hat{\rho}_{\min}$	r
Covariance	0.110	0.445	0.445	0.868	0.037	0.008	0.008	1
Correlation	0.255	0.348	0.397	0.651	0.463	0.320	0.320	1

Notes: The table reports estimated similarity scores ($\hat{\omega}_C, \hat{\omega}_F, \hat{\omega}_S$) and projection-residual diagnostics ($\hat{\rho}_C, \hat{\rho}_F, \hat{\rho}_S, \hat{\rho}_{\min}$) using residuals from the industry-level Fama–French regression in (3). The covariance operator preserves scale differences across industries, while the correlation operator normalizes industry-specific residual volatility. The similarity scores are relative geometric proximity measures and should not be interpreted as additive variance shares. The residual diagnostics measure absolute distance from the empirical operator to each covariance geometry.

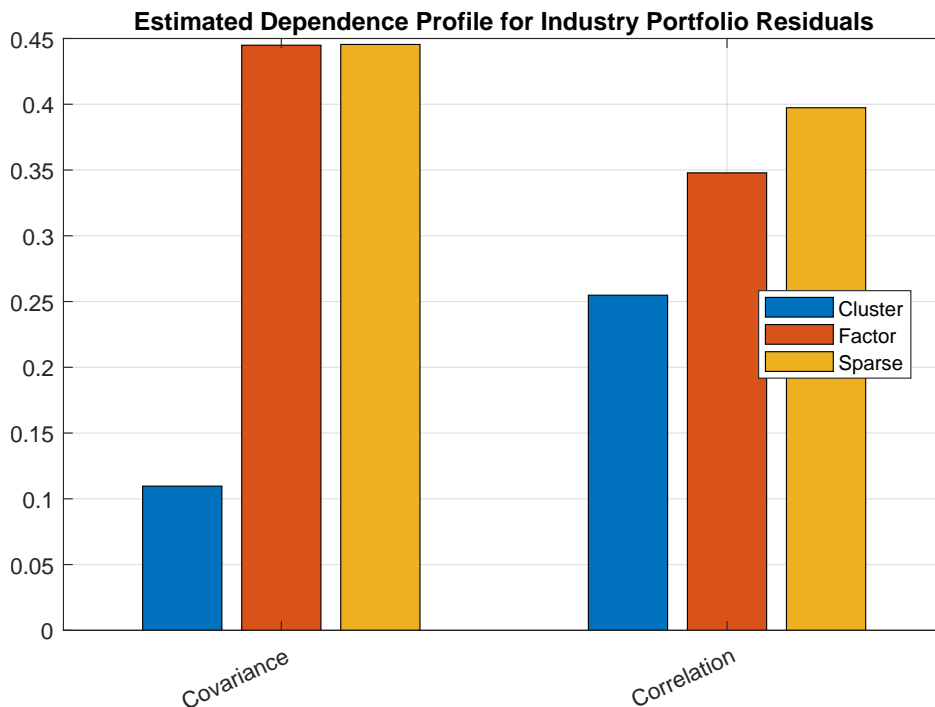


Figure 4: Estimated Dependence Profile for Industry Portfolio Residuals

Notes: The figure displays the estimated dependence profile based on the residual dependence operator. Each bar reports the relative geometric affinity of the empirical operator to the cluster, factor, and sparse covariance geometries. The corresponding projection-residual diagnostics are reported in Table 4.

Table 4 reveals a hybrid dependence structure.

Covariance operator. The factor and sparse scores are tied at $\hat{\omega}_F = \hat{\omega}_S = 0.445$, with a small cluster score $\hat{\omega}_C = 0.110$. The minimum projection residual $\hat{\rho}_{\min} = 0.008$ indicates that the sparse projection provides a near-perfect absolute fit to the residual covariance operator. Taken together, these findings indicate that residual co-movement among the 49 industry portfolios—after removing the three Fama–French factors—is concentrated in a

Table 5: Conventional Robust Standard Errors

Coefficient	Estimate	White	Sector cluster	Two-way cluster	Common-shock adj.
Intercept	-0.0485	0.0009	0.0141	0.0142	0.0002
MKT	0.9146	0.0220	0.0507	0.0603	0.0070
SMB	0.2393	0.0386	0.0578	0.0774	0.0143
HML	0.0565	0.0358	0.0745	0.0857	0.0132

Notes: The table reports coefficient estimates and standard errors for the pooled factor regression in (6). The columns compare heteroskedasticity-robust standard errors, sector-clustered standard errors, two-way clustered standard errors, and common-shock adjusted standard errors. The comparison illustrates how the estimated dependence profile can guide the interpretation of conventional robust inference procedures.

sparse set of industry pairs rather than being driven by broad industry-sector clustering. The small $\hat{\rho}_{\min}$ confirms that the sparse geometry adequately captures this residual dependence in an absolute sense. The non-negligible factor score suggests that some low-rank common component remains in the residuals despite the three-factor adjustment; this is consistent with known limitations of the Fama–French model as a complete description of common risk.

Correlation operator. Normalizing by industry volatility shifts the profile toward sparse dominance ($\hat{\omega}_S = 0.397$) with a moderate cluster score ($\hat{\omega}_C = 0.255$) and $\hat{\rho}_{\min} = 0.320$. The larger minimum residual indicates that the correlation structure is less well captured by the candidate geometries than the covariance structure, suggesting that industry-level volatility differences mask some localized dependence that only emerges after scale normalization.

Standard errors. Table 5 shows that sector-clustered standard errors are roughly $2.3\times$ the White standard errors for the market factor (0.051 vs. 0.022), and two-way clustered standard errors are slightly larger still (0.060). The common-shock adjusted standard errors are substantially smaller (0.007), reflecting the removal of the residual common factor component. These patterns are consistent with the estimated profile: the hybrid factor–sparse dependence structure implies that sector clustering overstates the within-cluster dependence, while the residual common component—identified by the factor score—is better absorbed by a common-shock adjustment than by clustering.

Procedure confidence index and inference recommendation. Table 6 reports the procedure confidence index $\hat{\kappa}$ and the profile-guided inference recommendation for each dependence operator.

Both operators yield small values of $\hat{\kappa}$. For the covariance operator, the factor and sparse scores are exactly tied at 0.445, so $\hat{\Delta}_\omega = 0$ and $\hat{\kappa} = 0$: the profile provides no statistical basis for preferring any single robust procedure. For the correlation operator, the sparse score marginally dominates ($\hat{\omega}_S = 0.397$), but the separation margin is only $\hat{\Delta}_\omega = 0.050$ and the minimum residual is $\hat{\rho}_{\min} = 0.320$, giving $\hat{\kappa} = 0.034$.

Table 6: Profile-Guided Inference Recommendation for Industry Portfolio Residuals

Operator	$\hat{\Delta}_\omega$	$\hat{\rho}_{\min}$	$\hat{\kappa}$	Dominant geometry	Profile-guided recommendation
Covariance	0.001	0.008	0.001	Sparse	Hybrid: report multiple SEs (low $\hat{\kappa}$)
Correlation	0.050	0.320	0.034	Sparse	Hybrid: report multiple SEs (low $\hat{\kappa}$)

Notes: The table reports the separation margin $\hat{\Delta}_\omega = \max_d \hat{\omega}_d - \max_{d \neq \hat{d}} \hat{\omega}_d$, the minimum projection residual $\hat{\rho}_{\min}$, the procedure confidence index $\hat{\kappa} = (1 - \hat{\rho}_{\min}) \hat{\Delta}_\omega$, the estimated dominant geometry, and the implied profile-guided recommendation. A small $\hat{\kappa}$ indicates either near-tie separation or poor dictionary fit; the recommended response is to report inference from multiple procedures.

These low confidence-index values have a clear practical implication: they correctly indicate that the empirical dependence structure is genuinely hybrid, and that no single inference procedure can be recommended with high confidence based on the data alone. The appropriate response—which the framework prescribes directly—is to report inference results from multiple procedures and document sensitivity to the choice. Table 5 operationalises this recommendation: the common-shock adjusted standard errors (appropriate when factor dependence is present) and the sector-clustered standard errors (appropriate when cluster dependence dominates) differ by a factor of approximately $7\times$ for the market factor, confirming that the choice of procedure is empirically consequential.

This example illustrates a key advantage of the proposed framework over a priori procedure selection. A researcher who assumes cluster dependence and uses sector-clustered standard errors is implicitly claiming $\hat{\kappa} \approx 1$ for the cluster geometry—a claim the data refute. A researcher who learns the profile first discovers the hybrid structure, obtains $\hat{\kappa} \approx 0$, and is correctly directed to report multiple procedures rather than to commit to one. The framework thus transforms an informal sensitivity analysis into a statistically grounded diagnostic.

9.6 Replication Details

The empirical illustration uses publicly available industry portfolio returns and factor data from Kenneth French’s Data Library. The replication package downloads the data, constructs excess returns, estimates (3), computes the empirical dependence operators in (4) and (5), estimates dependence profiles and projection-residual diagnostics, and generates Tables 4 and 5 and Figure 4.

All data transformations, sector mappings, parameter choices, and random seeds used in the empirical illustration are documented in the replication files.

10 Conclusion

This paper develops a framework for learning dependence structures from empirical measures of dependence. Rather than treating dependence structures as maintained assumptions, we view cluster, factor, and sparse dependence as covariance geometries and measure their proximity to an empirical dependence operator.

The proposed dependence profile provides a low-dimensional summary of high-dimensional dependence. We establish identification and estimation results for dependence profiles, introduce projection-residual diagnostics that assess the adequacy of the covariance dictionary, and develop a statistical theory for dependence classification. The analysis also characterizes ambiguous dependence structures through local alternatives and an indistinguishability result based on tangent-space overlap, showing that distinct dependence mechanisms may generate asymptotically indistinguishable similarity scores, thereby inducing classification uncertainty.

The framework delivers a concrete applied payoff. Proposition 4 shows that the profile-guided variance estimator $\widehat{V}^* = \widehat{V}_d$ is consistent under the dominant geometry, and the simulation experiment confirms that following the profile’s recommendation substantially reduces over-rejection relative to a default White HC estimator—from approximately 80% to near-nominal levels for the cluster DGP and substantially below 80% for the factor DGP. The profile therefore answers the applied question directly: a researcher who learns $(\widehat{\omega}_C, \widehat{\omega}_F, \widehat{\omega}_S)$ and applies the corresponding robust procedure achieves better-sized inference than one who applies an arbitrary correction.

More broadly, the paper suggests a geometric perspective in which dependence structures become objects of statistical learning rather than maintained assumptions, and dependence learning is governed by a geometric identification problem: positive principal angles permit learning, whereas tangent-space overlap creates fundamental ambiguity.

Future research may extend the covariance dictionary to additional dependence geometries, develop optimal profile-weighted combinations of robust procedures in the spirit of Hansen (2007), and establish the formal rate properties of the profile-guided estimator under local misspecification.

References

P.-A. Absil, Robert Mahony, and Rodolphe Sepulchre. *Optimization Algorithms on Matrix Manifolds*. Princeton University Press, Princeton, 2008.

- Donald W. K. Andrews. Heteroskedasticity and autocorrelation consistent covariance matrix estimation. *Econometrica*, 59(3):817–858, 1991.
- Manuel Arellano. Computing robust standard errors for within-groups estimators. *Oxford Bulletin of Economics and Statistics*, 49(4):431–434, 1987.
- Eric Auerbach. Identification and estimation of a partially linear regression model using network data. *Econometrica*, 87(3):931–980, 2019.
- Jushan Bai. Inferential theory for factor models of large dimensions. *Econometrica*, 71(1):135–171, 2003.
- Jushan Bai and Serena Ng. Determining the number of factors in approximate factor models. *Econometrica*, 70(1):191–221, 2002.
- J. M. Bates and C. W. J. Granger. The combination of forecasts. *Operational Research Quarterly*, 20(4):451–468, 1969.
- Claude Berge. *Topological Spaces*. Oliver and Boyd, Edinburgh, 1963. Translated from the French by E. M. Patterson. Original: *Espaces Topologiques, Fonctions Multivoques*, Dunod, Paris, 1959.
- Peter J. Bickel and Elizaveta Levina. Covariance regularization by thresholding. *Annals of Statistics*, 36(6):2577–2604, 2008.
- Peter J. Bickel, Chris A. J. Klaassen, Ya’acov Ritov, and Jon A. Wellner. *Efficient and Adaptive Estimation for Semiparametric Models*. Johns Hopkins University Press, Baltimore, 1993.
- T. Tony Cai and Weidong Liu. Adaptive thresholding for sparse covariance matrix estimation. *Journal of the American Statistical Association*, 106(494):672–684, 2011.
- A. Colin Cameron and Douglas L. Miller. A practitioner’s guide to cluster-robust inference. *Journal of Human Resources*, 50(2):317–372, 2015.
- A. Colin Cameron, Jonah B. Gelbach, and Douglas L. Miller. Robust inference with multiway clustering. *Journal of Business & Economic Statistics*, 29(2):238–249, 2011.
- Emmanuel J. Candès, Xiaodong Li, Yi Ma, and John Wright. Robust principal component analysis? *Journal of the ACM*, 58(3):1–37, 2011.
- Gary Chamberlain and Michael Rothschild. Arbitrage, factor structure, and mean-variance analysis on large asset markets. *Econometrica*, 51(5):1281–1304, 1983.

- Venkat Chandrasekaran, Pablo A. Parrilo, and Alan S. Willsky. Rank-sparsity incoherence for matrix decomposition. *SIAM Journal on Optimization*, 21(2):572–596, 2011.
- Timothy G. Conley. GMM estimation with cross sectional dependence. *Journal of Econometrics*, 92(1):1–45, 1999.
- Timothy G. Conley. Spatial econometrics. In *The New Palgrave Dictionary of Economics*. Palgrave Macmillan, London, 2 edition, 2008.
- Frank Deutsch. *Best Approximation in Inner Product Spaces*. Springer, New York, 2001.
- John C. Driscoll and Aart C. Kraay. Consistent covariance matrix estimation with spatially dependent panel data. *Review of Economics and Statistics*, 80(4):549–560, 1998.
- Eugene F. Fama and Kenneth R. French. Common risk factors in the returns on stocks and bonds. *Journal of Financial Economics*, 33(1):3–56, 1993.
- Kenneth R. French. Kenneth R. french data library. https://mba.tuck.dartmouth.edu/pages/faculty/ken.french/data_library.html, 2025. Accessed June 2025.
- Jerome Friedman, Trevor Hastie, and Robert Tibshirani. Sparse inverse covariance estimation with the graphical Lasso. *Biostatistics*, 9(3):432–441, 2008.
- Bruce E. Hansen. Least squares model averaging. *Econometrica*, 75(4):1175–1189, 2007.
- Lucien Le Cam and Grace Lo Yang. *Asymptotics in Statistics: Some Basic Concepts*. Springer, New York, 2 edition, 2000.
- Michael P. Leung. Causal inference under approximate neighborhood interference. *Econometrica*, 90(1):267–293, 2022.
- Adrian S. Lewis and Jérôme Malick. Alternating projections on manifolds. *Mathematics of Operations Research*, 33(1):216–234, 2008.
- Kung-Yee Liang and Scott L. Zeger. Longitudinal data analysis using generalized linear models. *Biometrika*, 73(1):13–22, 1986.
- Whitney K. Newey. The asymptotic variance of semiparametric estimators. *Econometrica*, 62(6):1349–1382, 1994.
- Whitney K. Newey and Kenneth D. West. A simple, positive semi-definite, heteroskedasticity and autocorrelation consistent covariance matrix. *Econometrica*, 55(3):703–708, 1987.

R. Tyrrell Rockafellar and Roger J.-B. Wets. *Variational Analysis*. Springer, Berlin, 1998.

Aad W. van der Vaart and Jon A. Wellner. *Weak Convergence and Empirical Processes*. Springer, New York, 1996.

Halbert White. A heteroskedasticity-consistent covariance matrix estimator and a direct test for heteroskedasticity. *Econometrica*, 48(4):817–838, 1980.

Online Appendix for “Learning Dependence Structures for Econometric Inference”

A Additional Results for Geometric Identification

A.1 Regular Points and Tangent Spaces

We introduce explicit regularity conditions for each geometry and derive the associated tangent spaces.

Cluster geometry. Let \mathcal{I}_C be the cluster support set defined in Section 2. A point $\Sigma_C \in \mathcal{S}_C$ is *regular* if $(\Sigma_C)_{ab} \neq 0$ for every $(a, b) \in \mathcal{I}_C$. Under this condition, the active support pattern is locally stable: any Σ sufficiently close to Σ_C has the same support \mathcal{I}_C . The tangent space at a regular cluster point Σ_C is the closed linear subspace

$$T_C(\Sigma_C) = \{H \in \mathbb{H} : H_{ab} = 0 \text{ whenever } (a, b) \notin \mathcal{I}_C\}.$$

Tangent directions may perturb any covariance entry on the cluster support but cannot introduce dependence between observations sharing no cluster membership.

Factor geometry. Write $\Sigma_F = L_0 + D_0$ with $L_0 = \Lambda_0 \Lambda_0'$, $\text{rank}(L_0) = r$, and D_0 diagonal. A point Σ_F is *regular* if the r leading eigenvalues of L_0 are positive and distinct. Under this generic condition the rank- r manifold is smooth at L_0 (Lewis and Mallick, 2008), and the tangent space of $\mathcal{S}_F(r)$ at Σ_F is

$$T_F(\Sigma_F) = \{\Lambda_0 H' + H \Lambda_0' + \text{diag}(v) : H \in \mathbb{R}^{n \times r}, v \in \mathbb{R}^n\}.$$

The first two terms span the tangent of the rank- r manifold at L_0 ; the diagonal term $\text{diag}(d)$ accounts for free perturbations of the noise floor D_0 . Note that $\mathcal{S}_F(r)$ is a cone: if $\Gamma = L + D \in \mathcal{S}_F(r)$ then $a\Gamma = aL + aD \in \mathcal{S}_F(r)$ for all $a > 0$, since $\text{rank}(aL) = \text{rank}(L) \leq r$ and aD is diagonal.

Sparse geometry. Let $\mathcal{I}_S = \text{supp}(\Sigma_S)$ with $|\mathcal{I}_S| \leq k_n$. A point Σ_S is *regular* if the k_n -th and $(k_n + 1)$ -th largest absolute off-diagonal entries of Σ_S are distinct. This ensures local

uniqueness of the sparse projection. The tangent space at a regular sparse point is

$$T_S(\Sigma_S) = \{H \in \mathbb{H} : H_{ij} = 0 \text{ whenever } (i, j) \notin \mathcal{I}_S\}.$$

The diagonal is a common nuisance direction. By construction, $(i, i) \in \mathcal{I}_C$ for every i (every observation trivially shares a cluster membership with itself), so $\text{diag}(v) \in T_C(\Sigma_C)$ for every $v \in \mathbb{R}^n$: the cluster tangent space contains *all* diagonal perturbations. The factor tangent space $T_F(\Sigma_F)$ contains the same set of diagonal perturbations directly, via its free $\text{diag}(v)$ term, which represents the noise floor D_0 . Consequently,

$$\{\text{diag}(v) : v \in \mathbb{R}^n\} \subseteq T_C(\Sigma_C) \cap T_F(\Sigma_F)$$

at *every* pair of regular cluster and factor points, regardless of parameter values: the cluster and factor tangent spaces always share the full diagonal subspace. This is a substantive feature of the geometries, not an estimation artifact, and it reflects the fact that all three covariance classes leave each observation’s own variance (Σ_{ii}) unrestricted; the diagonal is a common nuisance direction present in every geometry under consideration; analogously, the sparse projection of Section B.1 always retains the diagonal regardless of the sparsity budget k_n . Because the diagonal carries no information about *dependence* between distinct observations—which is the object of interest throughout this paper—we factor it out of the principal-angle condition below by restricting attention to the off-diagonal part of each tangent space,

$$T_d^{\text{off}}(\Sigma_d) = \{H \in T_d(\Sigma_d) : H_{ii} = 0 \text{ for all } i\}, \quad d \in \mathcal{D}.$$

Equivalently, $T_d^{\text{off}}(\Sigma_d)$ is the intersection of $T_d(\Sigma_d)$ with the off-diagonal hyperplane $\{H \in \mathbb{H} : \text{diag}(H) = 0\}$; for the cluster and sparse geometries this simply removes the diagonal entries from the coordinate subspace $T_d(\Sigma_d)$, and for the factor geometry it removes the $\text{diag}(d)$ term entirely, since $\Lambda_0 H' + H \Lambda_0' + \text{diag}(v)$ has zero off-diagonal contribution from $\text{diag}(v)$.

A.2 Principal-Angle Condition

Remark A.1 (Why the Off-Diagonal Restriction Is Necessary). *Assumption 1 is stated in terms of the off-diagonal tangent spaces T_d^{off} introduced in Section A.1, rather than the full tangent spaces T_d . This restriction is not a matter of convenience: as shown there, $T_C(\Sigma_C) \cap T_F(\Sigma_F)$ always contains the entire diagonal subspace $\{\text{diag}(v) : v \in \mathbb{R}^n\}$, for every pair of*

regular cluster and factor points and every parameter configuration, so $\theta(T_C(\Sigma_C), T_F(\Sigma_F)) = 0$ identically and Assumption 1 stated with the unrestricted tangent spaces could never hold for the cluster–factor pair. This reflects the fact that own-variance perturbations are common to every covariance geometry considered in this paper and carry no information distinguishing one dependence geometry from another. Restricting to the off-diagonal directions T_d^{off} isolates exactly the perturbations that are informative about dependence, which is the relevant object of identification.

The next lemma isolates the role of within-class regularity: at a regular point of a given geometry, the projection onto *that* geometry alone is locally single-valued. This conclusion uses only the regularity conditions of Section A.1 and does not yet involve the relationship between different geometries.

Lemma A.5 (Local Uniqueness of Individual Projections). *Suppose Σ_C , Σ_F , and Σ_S are regular points of \mathcal{S}_C , $\mathcal{S}_F(r)$, and \mathcal{S}_S , respectively, in the sense of Section A.1. Then P_C is locally single-valued at Σ_C , P_F is locally single-valued at Σ_F , and P_S is locally single-valued at Σ_S .*

Local uniqueness of each projection is necessary for the dependence profile to be well defined near Σ_0 , but it is not sufficient for the profile to carry separate information about cluster, factor, and sparse geometry: if two tangent spaces shared a common direction, a perturbation along that direction would move *both* projections in a coupled way, and the resulting change in the profile could not be uniquely attributed to either geometry. The principal-angle condition rules this out by ensuring that the tangent spaces of distinct geometries intersect only at the origin.

Diagonal perturbations are never separately identified By Section A.1, every diagonal perturbation $\text{diag}(d)$ lies in $T_C(\Sigma_C) \cap T_F(\Sigma_F)$ (and, since the sparse projection of Section B.1 always retains the diagonal, in $T_S(\Sigma_S)$ as well), regardless of the principal-angle condition. Consequently, a perturbation of Γ_0 confined to its own diagonal—that is, a change in observation-specific variances with no change in any cross-covariance—cannot be attributed to cluster, factor, or sparse dependence: it is consistent with all three geometries simultaneously and with none of them specifically. This is not a defect of Assumption 1 or of Theorem 1; it reflects the fact that the dependence profile is, by design, a summary of off-diagonal dependence structure. Variance heterogeneity across observations is a separate object, already well studied under the heading of heteroskedasticity, and is intentionally outside the scope of dependence learning as formulated here.

A.3 Ambiguous Dependence Structures

The principal-angle condition ensures local separation between covariance geometries along off-diagonal directions. When this separation breaks down and off-diagonal tangent spaces overlap, ambiguity may arise as a fundamental feature of the problem rather than a consequence of limited sample size. The following result formalizes this local indistinguishability phenomenon.

Identification versus Ambiguity Theorems 1 and 2 characterize the boundary between identifiable and ambiguous dependence structures. Positive principal angles ensure local separation of covariance geometries and hence local identifiability of the dependence profile. Conversely, overlapping tangent spaces generate local indistinguishability, so that ambiguity reflects a fundamental lack of identifying information rather than finite-sample uncertainty. Thus, identification and indistinguishability represent two sides of the same geometric phenomenon.

A.4 Examples of Geometric Overlap

Three further situations produce overlap between covariance geometries along off-diagonal directions, in addition to the unconditional diagonal overlap of Remark A.2.

Cluster-sparse overlap. A one-way cluster covariance matrix with G balanced groups of size n/G has a block-support of size $G \cdot (n/G)^2$. When $G \cdot (n/G)^2 = O(k_n)$, the cluster support is no larger than the sparse budget k_n , so the cluster geometry lies inside the sparse class. In such cases $T_C(\Sigma_C) \subseteq T_S(\Sigma_C)$ and the principal angle $\theta(T_C, T_S)$ can be arbitrarily small.

Two-way cluster-sparse overlap. Consider observations indexed by firm $i = 1, \dots, N$ and period $t = 1, \dots, T$, with two-way cluster dependence $\text{Cov}(u_{it}, u_{js}) \neq 0$ whenever $i = j$ or $t = s$. The non-zero support has two parts: NT^2 within-firm entries (same firm, any two periods) and $TN^2 - NT$ cross-period entries (different firms, same period). For the baseline parameters $N = 25$, $T = 10$, these are 2,500 and 6,000 entries respectively, out of $n^2 = 62,500$ total.

A one-way industry cluster projection captures the 2,500 within-firm entries but misses the 6,000 cross-period entries entirely, leaving a non-trivial projection residual. The sparse projection retains the k_n largest off-diagonal entries in absolute value, which include many of the cross-period entries that the cluster projection cannot reach. As a result, the cluster and sparse scores are simultaneously large under two-way clustering: the cluster score reflects within-industry co-movement, while the sparse score captures the additional cross-period

co-movement that falls outside the one-way cluster support. This explains why the dependence profile does not collapse to a single dominant geometry under two-way clustering, and illustrates the usefulness of reporting the full profile rather than a binary classification.

Cluster-factor overlap. Two distinct mechanisms can drive overlap between the cluster and factor geometries. The first is unconditional: as established in Section A.1 and Remark A.2, $T_C(\Sigma_C)$ and $T_F(\Sigma_F)$ always share the diagonal subspace, so $\theta(T_C, T_F) = 0$ exactly whenever the principal angle is computed without the off-diagonal restriction; this is why Assumption 1 is stated for T_C^{off} and T_F^{off} rather than T_C and T_F . The second mechanism is parameter-dependent and genuinely off-diagonal: a block-diagonal covariance matrix with a small number of large, homogeneous blocks has a leading eigenvalue of order n/G and is also well approximated by a rank-one factor structure, so the off-diagonal parts of T_C and T_F may themselves nearly align for such designs. Both mechanisms produce overlap that is intrinsic to the problem rather than a failure of the proposed method, but only the second is sensitive to parameter choices such as the number and size of clusters; the first holds for every cluster and factor geometry considered in this paper.

A Additional Results for Dependence Operator

B.1 Computational Implementation

Given $\widehat{\Gamma}_n$, define the empirical projection onto geometry $d \in \mathcal{D}$ by

$$\widehat{P}_d = P_d(\widehat{\Gamma}_n).$$

This subsection describes practical implementations of the cluster, factor, and sparse projections.

Cluster Projection. Using the cluster-support matrix M_C defined in Section 2, the cluster projection is

$$\widehat{P}_C = M_C \odot \widehat{\Gamma}_n,$$

where \odot denotes the Hadamard product. This removes covariance entries incompatible with the cluster structure and preserves entries between observations sharing at least one cluster membership. When cluster memberships are unknown, they may be estimated via spectral clustering, community-detection methods, or latent-group estimators before constructing M_C .

Factor Projection. The factor class $\mathcal{S}_F(r) = \{\Gamma \succeq 0 : \Gamma = L + D, \text{rank}(L) \leq r, D \text{ diagonal}\}$ requires separating $\widehat{\Gamma}_n$ into a low-rank component L and a diagonal component D . We compute this projection via the following alternating-projection algorithm, which is the analogue of the principal-factor (minres) algorithm in classical factor analysis.

1. **Initialise.** Set $D^{(0)} = \text{diag}(\widehat{\Gamma}_n)$.
2. **Low-rank step.** For $k = 0, 1, 2, \dots$, compute the rank- r positive-semidefinite truncation of $\widehat{\Gamma}_n - D^{(k)}$:

$$L^{(k+1)} = \widehat{U}_r^{(k)} \max(\widehat{\Lambda}_r^{(k)}, 0) (\widehat{U}_r^{(k)})',$$

where $\widehat{U}_r^{(k)}$ and $\widehat{\Lambda}_r^{(k)}$ contain the r leading eigenvectors and eigenvalues of $\widehat{\Gamma}_n - D^{(k)}$.

3. **Diagonal step.** Set

$$d_i^{(k+1)} = (\widehat{\Gamma}_n)_{ii} - L_{ii}^{(k+1)}, \quad i = 1, \dots, n,$$

so that $D^{(k+1)} = \text{diag}(d^{(k+1)})$. If $\lambda_{\min}(L^{(k+1)} + D^{(k+1)}) < 0$, replace

$$d_i^{(k+1)} \leftarrow d_i^{(k+1)} + (-\lambda_{\min}(L^{(k+1)} + D^{(k+1)}) + \varepsilon), \quad i = 1, \dots, n,$$

for a small tolerance $\varepsilon > 0$. This shift is applied only when the matrix is not positive semidefinite; it guarantees $L^{(k+1)} + D^{(k+1)} \succeq 0$ and leaves the objective unchanged when no shift is needed.

4. **Converge.** Stop when $\max_i |D_{ii}^{(k+1)} - D_{ii}^{(k)}| < \delta$ for a tolerance $\delta > 0$.

Each step reduces the Frobenius objective $\|\widehat{\Gamma}_n - L - D\|_F^2$ monotonically. The algorithm converges in practice in fewer than 20 iterations for the covariance matrices arising in the simulation designs. The output is

$$\widehat{P}_F = L^* + D^*,$$

where (L^*, D^*) denote the values at convergence.

The factor rank r may be selected using information criteria, eigenvalue-ratio methods, scree-plot procedures, or other standard techniques from the factor-model literature.

Population projection versus computational algorithm. Throughout the paper, P_F denotes the population projection operator onto \mathcal{S}_F , defined as the Frobenius-norm minimizer over the (nonconvex) class $\mathcal{S}_F(r)$. The alternating-projection algorithm above is a computational heuristic for approximating this minimizer; each step is monotone in the

Frobenius objective, so the algorithm converges to a stationary point, but because $\mathcal{S}_F(r)$ is nonconvex this stationary point need not be the global minimizer $P_F(\widehat{\Gamma}_n)$ except when $\widehat{\Gamma}_n$ is sufficiently close to a regular factor point and the algorithm is initialized appropriately (e.g., as in step 1). This mirrors the local-uniqueness result of Lemma A.5: local identification of the factor projection is established at regular points, while global identification of P_F away from such points is not claimed and is not required for the asymptotic theory of Sections 3–5, which is stated entirely in terms of local properties of Γ_0 . In the simulation and empirical exercises of Sections 8–9, the diagonal initialization in step 1 combined with a clear eigenvalue gap (verified informally via the eigenvalue-ratio criterion of Section B.1) makes convergence to the population projection plausible, but this is a numerical observation rather than a proven global guarantee.

Sparse Projection. The sparse projection may be obtained through hard thresholding, soft thresholding, or sparse optimization. For example, under hard thresholding,

$$(\widehat{P}_S)_{ij} = \widehat{\Gamma}_{n,ij} \mathbf{1}\{|\widehat{\Gamma}_{n,ij}| > \tau_n\},$$

where τ_n is a threshold sequence. More generally, one may compute

$$\widehat{P}_S = \arg \min_{\Gamma \in \mathbb{H}} \left\{ \|\widehat{\Gamma}_n - \Gamma\|_F^2 + \lambda_n \|\Gamma\|_1 \right\}.$$

Thresholding preserves entries exhibiting sufficiently strong dependence while removing weak interactions. The resulting estimator can be interpreted as a sparse approximation to the empirical dependence operator.

Computational Complexity. Among the three projections, the factor projection is typically the most computationally demanding. Each iteration of the alternating-projection algorithm requires one eigendecomposition of an $n \times n$ matrix, costing $O(n^3)$ operations. Because the algorithm converges rapidly (typically fewer than 20 iterations), the total cost is $O(Kn^3)$ where K denotes the number of iterations. Randomized and truncated eigendecomposition algorithms can substantially reduce this cost in large-scale applications.

The cluster projection requires construction of the cluster-support matrix M_C . Given cluster memberships, this operation is typically of order $O(Mn^2)$, where M denotes the number of clustering dimensions. The subsequent Hadamard projection is of order $O(n^2)$.

Sparse projections obtained by thresholding are also of order $O(n^2)$, while optimization-based sparse projections may require additional iterative computations depending on the algorithm employed.

Unknown geometric specifications. The discussion above assumes that the cluster partition, factor rank, and sparsity level are specified. In practice, these quantities may themselves be estimated from the data. The statistical analysis in this paper treats these geometric specifications as given and focuses on learning the relative similarity of the empirical dependence operator to the resulting covariance geometries. Joint estimation of dependence geometries and dependence profiles is an important direction for future research.

B.2 Additional Choice of Dependence Operator

Different empirical operators emphasize different aspects of dependence and may therefore produce different dependence profiles. Consequently, the estimated dependence profile should be interpreted relative to the dependence operator from which it is constructed.

Long-Run Covariance Operators. For time-series or panel applications with serial dependence, a more appropriate choice is often a long-run covariance operator,

$$\hat{\Gamma}_n = \sum_{|h| \leq L} K\left(\frac{h}{L}\right) \hat{\Gamma}(h),$$

where $\hat{\Gamma}(h)$ denotes a sample autocovariance operator, $K(\cdot)$ is a kernel function, and L is a bandwidth parameter. Such operators emphasize persistent temporal dependence and form the basis of heteroskedasticity and autocorrelation consistent estimation (Newey and West, 1987; Andrews, 1991).

Spatial Covariance Operators. When observations possess geographical locations, distance-weighted covariance operators often provide a more informative description of dependence. A generic spatial covariance operator is

$$\hat{\Gamma}_n = \left[K\left(\frac{d_{ij}}{b_n}\right) \hat{u}_i \hat{u}_j \right]_{i,j=1}^n,$$

where d_{ij} denotes the geographical distance between observations i and j , $K(\cdot)$ is a spatial kernel, and b_n is a distance bandwidth. Such operators arise naturally in the spatial HAC literature and assign larger weights to nearby observations than to distant observations (Conley, 1999, 2008). When dependence is generated by local geographical interactions, spatial covariance operators may reveal dependence patterns that are not apparent from the unweighted covariance operator alone.

Network Dependence Operators. For network data, dependence may be encoded through an adjacency matrix $A = (A_{ij})$. A natural network dependence operator is

$$\widehat{\Gamma}_n = A \odot (\widehat{u}\widehat{u}'),$$

where \odot denotes the Hadamard product. This operator concentrates attention on dependence among economically connected units and is useful when interactions are generated by production networks, social networks, financial linkages, or other forms of economic connectivity (Auerbach, 2019; Leung, 2022).

Cluster-Based Covariance Operators. When cluster memberships are known, one may construct a cluster-supported covariance operator of the form

$$\widehat{\Gamma}_n^{(C)} = M_C \odot \widehat{\Gamma}_n,$$

where \odot denotes the Hadamard product and M_C is the cluster-support matrix.

Using the cluster-support matrix M_C defined in Section 2, the cluster-based operator retains covariance entries consistent with the assumed clustering structure while setting cross-cluster entries to zero. This construction accommodates one-way, two-way, and multi-way clustering as special cases. It is particularly useful when the objective is to isolate the structured-support pattern generated by cluster dependence and distinguish it from alternative dependence geometries such as factor or sparse dependence.

Discussion. The purpose of dependence learning is not to recover a single universal dependence profile. Rather, the profile summarizes the geometry of dependence encoded in a chosen population dependence operator. The choice of operator should therefore be guided by economic theory, institutional knowledge, sampling design, and the particular inferential objective under consideration.

In this sense, dependence learning should be viewed as a second-stage dimension-reduction problem applied to an estimated dependence operator.

A Proofs of the Main Results

C.1 Proofs of Results in Section 3

This subsection contains the proofs of Lemmas 1, 2, and 3, together with the proofs of Theorems 1 and 2.

Proof of Lemma 1. Let $f(\Gamma) = \|\Sigma - \Gamma\|_F$. Since f is continuous and \mathcal{S}_D is closed in finite-dimensional \mathbb{H} , every minimizing sequence has a convergent subsequence with limit in \mathcal{S}_D . The limit attains the infimum. \square

Proof of Lemma 2. The objective $f(\Sigma, \Gamma) = \|\Sigma - \Gamma\|_F$ is jointly continuous. Since \mathcal{S}_D is closed, the argmin correspondence $\Sigma \mapsto \arg \min_{\Gamma \in \mathcal{S}_D} \|\Sigma - \Gamma\|_F$ is upper hemicontinuous by the maximum theorem of Berge (1963). Under local uniqueness, this correspondence is single-valued in a neighborhood of Σ , so the selection P_D is a continuous function there. \square

Proof of Lemma 3. (\Leftarrow) Suppose $U \cap V = \{0\}$. The function $(u, v) \mapsto \langle u, v \rangle_F / (\|u\|_F \|v\|_F)$ is continuous on the set $\{(u, v) \in U \times V : \|u\|_F = \|v\|_F = 1\}$, which is the intersection of the unit spheres of U and V and is compact (closed and bounded in finite-dimensional \mathbb{H}). If $\theta(U, V) = 0$, there exist sequences $u_m \in U$, $v_m \in V$ with $\|u_m\|_F = \|v_m\|_F = 1$ and $\langle u_m, v_m \rangle_F \rightarrow 1$. By compactness, passing to a subsequence, $u_m \rightarrow u^* \in U$ and $v_m \rightarrow v^* \in V$ with $\|u^*\|_F = \|v^*\|_F = 1$ and $\langle u^*, v^* \rangle_F = 1$. By the Cauchy–Schwarz equality case, $u^* = v^*$, so $u^* \in U \cap V$ with $u^* \neq 0$, contradicting $U \cap V = \{0\}$. Hence $\theta(U, V) > 0$.

(\Rightarrow) Suppose $U \cap V \neq \{0\}$, and let $w \in U \cap V$ with $w \neq 0$. Taking $u = v = w/\|w\|_F$ gives $\langle u, v \rangle_F = 1$, so $\theta(U, V) = \arccos(1) = 0$. \square

Proof of Theorem 1. Local uniqueness. By Lemma A.5, P_C , P_F , and P_S are each locally single-valued at the respective regular points $\Sigma_C, \Sigma_F, \Sigma_S$. By Lemma D.13, each P_D is locally Lipschitz, hence continuous. Since

$$\omega_D(\Sigma) = \frac{\|P_D(\Sigma)\|_F^2}{\sum_{D' \in \mathfrak{D}} \|P_{D'}(\Sigma)\|_F^2}$$

is a continuous function of the projections whenever the denominator $S_{T,0} > 0$, the dependence profile is locally identified as a continuous function of Σ .

Separated identification. It remains to show the stated separation property: no nonzero off-diagonal direction lies in more than one off-diagonal tangent space simultaneously. By Assumption 1, $\theta(T_i^{\text{off}}(\Sigma_i), T_j^{\text{off}}(\Sigma_j)) \geq \theta_0 > 0$ for all $i \neq j$ in $\{C, F, S\}$. By Lemma 3, this is equivalent to

$$T_i^{\text{off}}(\Sigma_i) \cap T_j^{\text{off}}(\Sigma_j) = \{0\}, \quad i \neq j.$$

Hence for any nonzero off-diagonal $H \in \mathbb{H}$ (i.e., $\text{diag}(H) = 0$), H cannot belong to two of $T_C^{\text{off}}(\Sigma_C)$, $T_F^{\text{off}}(\Sigma_F)$, $T_S^{\text{off}}(\Sigma_S)$ at once. Equivalently, a first-order off-diagonal perturbation $\Sigma_0 + tH + o(t)$ that is tangent to geometry i (i.e., $H \in T_i^{\text{off}}(\Sigma_i)$) cannot simultaneously be tangent to geometry $j \neq i$ unless $H = 0$. Since, at a regular point, the derivative of P_i in the direction $H \in T_i(\Sigma_i)$ coincides with the orthogonal projection of H onto $T_i(\Sigma_i)$

itself (the projection map acts as the identity to first order along its own tangent space), a nonzero off-diagonal perturbation that changes $S_i = \|P_i(\Sigma)\|_F^2$ to first order along $T_i^{\text{off}}(\Sigma_i)$ cannot, by the transversality just established, also change S_j to first order through the same off-diagonal direction for $j \neq i$. This is the precise sense in which the three similarity scores are separately, rather than confoundedly, identified near Σ_0 *along off-diagonal (dependence) directions*; by Remark A.2, no analogous separation holds, or is claimed, for diagonal (variance) perturbations. \square

Proof of Theorem 2. Step 1: LAN at Γ_0 . Under Assumption 3, for any bounded sequence $H_n \rightarrow H$,

$$\log \frac{dP_{\Gamma_0+n^{-1/2}H_n}^n}{dP_{\Gamma_0}^n} = \Delta_n(H) - \frac{1}{2}\|H\|_{\mathcal{I}}^2 + o_p(1), \quad (\text{C.1})$$

where $\Delta_n(H) = n^{-1/2} \sum_{i=1}^n \ell_i(H) \Rightarrow N(0, \|H\|_{\mathcal{I}}^2)$ under $P_{\Gamma_0}^n$.

Step 2: Identical log-likelihood ratios and contiguity. Because $\Gamma_{i,n}$ and $\Gamma_{j,n}$ share the same first-order local expansion $\Gamma_0 + n^{-1/2}H + o(n^{-1/2})$, applying (C.1) to both sequences yields

$$\log \frac{dP_{\Gamma_{i,n}}^n}{dP_{\Gamma_0}^n} - \log \frac{dP_{\Gamma_{j,n}}^n}{dP_{\Gamma_0}^n} = o_p(1) \quad \text{under } P_{\Gamma_0}^n.$$

Hence the log-likelihood ratio between the two experiments,

$$\Lambda_n = \log \frac{dP_{\Gamma_{i,n}}^n}{dP_{\Gamma_{j,n}}^n},$$

satisfies $\Lambda_n = o_p(1)$ under $P_{\Gamma_0}^n$. By LAN, the log-likelihood ratio $\log(dP_{\Gamma_{j,n}}^n/dP_{\Gamma_0}^n)$ converges in distribution under $P_{\Gamma_0}^n$ to $N(-\frac{1}{2}\|H\|_{\mathcal{I}}^2, \|H\|_{\mathcal{I}}^2)$, which implies that $P_{\Gamma_{j,n}}^n$ is contiguous with respect to $P_{\Gamma_0}^n$ (van der Vaart and Wellner, 1996, Lemma 6.4). By contiguity, $\Lambda_n = o_p(1)$ under $P_{\Gamma_0}^n$ implies $\Lambda_n = o_p(1)$ under $P_{\Gamma_{j,n}}^n$ (and, by the same argument applied to $\Gamma_{i,n}$, under $P_{\Gamma_{i,n}}^n$).

Step 3: Total variation convergence. By the Hellinger–total-variation inequality, for any two probability measures P and Q ,

$$\|P - Q\|_{\text{TV}} \leq \sqrt{1 - \exp(-H^2(P, Q))},$$

where $H^2(P, Q) = \frac{1}{2} \int (\sqrt{dP} - \sqrt{dQ})^2$ is the squared Hellinger distance. Since $\Lambda_n = o_p(1)$, a standard calculation gives $H^2(P_{\Gamma_{i,n}}^n, P_{\Gamma_{j,n}}^n) \rightarrow 0$ (van der Vaart and Wellner, 1996, Lemma 2.27). Therefore

$$\|P_{\Gamma_{i,n}}^n - P_{\Gamma_{j,n}}^n\|_{\text{TV}} \rightarrow 0.$$

Step 4: Test bound. For any test $\varphi_n \in [0, 1]$,

$$|E_{\Gamma_{i,n}}\varphi_n - E_{\Gamma_{j,n}}\varphi_n| \leq \|P_{\Gamma_{i,n}}^n - P_{\Gamma_{j,n}}^n\|_{\text{TV}} \rightarrow 0.$$

Hence no test can have asymptotic size tending to zero and power tending to one for distinguishing \mathcal{S}_i from \mathcal{S}_j along these local sequences. \square

C.2 Proofs of Results in Sections 4 and 5

This subsection contains the proofs of Proposition 1, Lemma 4, Corollary 1, and Theorems 3–4.

Proof of Proposition 1. By Lemma D.13, P_D is locally Lipschitz at Γ_0 for each $D \in \mathfrak{D}$. Since $\|\widehat{\Gamma}_n - \Gamma_0\|_F = o_p(1)$ by Assumption 4, it follows that $\|P_D(\widehat{\Gamma}_n) - P_D(\Gamma_0)\|_F = o_p(1)$. Continuity of the Frobenius norm then gives

$$\rho_D(\widehat{\Gamma}_n) = \frac{\|\widehat{\Gamma}_n - P_D(\widehat{\Gamma}_n)\|_F}{\|\widehat{\Gamma}_n\|_F} \xrightarrow{p} \frac{\|\Gamma_0 - P_D(\Gamma_0)\|_F}{\|\Gamma_0\|_F} = \rho_D(\Gamma_0).$$

The result for ρ_{\min} follows from the continuous mapping theorem applied to the minimum over a finite set. \square

Proof of Lemma 4. By local Lipschitz continuity,

$$\|\widehat{P}_D - P_D(\Gamma)\|_F \leq L_D \|\widehat{\Gamma}_n - \Gamma\|_F$$

with probability approaching one. Assumption 4 gives the result for each D . Since $\{C, F, S\}$ is finite, the maximum is also $o_p(1)$. \square

Proof of Theorem 3. By Lemma 4,

$$\widehat{P}_D - P_D(\Gamma) = o_p(1)$$

uniformly over D . Continuity of the Frobenius norm gives $\widehat{S}_D - S_D = o_p(1)$. Applying the continuous mapping theorem to $\widehat{\omega}_D = \widehat{S}_D / \widehat{S}_T$ gives $\widehat{\omega} - \omega = o_p(1)$. \square

Proof of Corollary 1. By Lemma D.7, each P_D is Hadamard differentiable at Γ_0 with derivative $DP_D(\Gamma_0)[H] = \Pi_{T_D(\Gamma_0)}(H)$. The map $g(P) = \|P\|_F^2 = \langle P, P \rangle_F$ is a quadratic form on the finite-dimensional space \mathbb{H} and is therefore Fréchet differentiable everywhere, with derivative $Dg(P)[K] = 2\langle P, K \rangle_F$. Since $S_D = g \circ P_D$, the chain rule for Hadamard-differentiable maps

composed with a Fréchet-differentiable map (van der Vaart and Wellner, 1996, Lemma 3.9.3) gives that S_D is Hadamard differentiable at Γ_0 , with derivative

$$\dot{S}_{D,\Gamma_0}[H] = Dg(P_D(\Gamma_0))[DP_D(\Gamma_0)[H]] = 2\langle P_D(\Gamma_0), \Pi_{T_D(\Gamma_0)}(H) \rangle_F.$$

Applying this to each $D \in \{C, F, S\}$ and stacking gives Hadamard differentiability of the vector-valued map $\mathcal{S}(\cdot)$, since a vector of Hadamard-differentiable real-valued maps is itself Hadamard differentiable (apply the definition coordinatewise along the same sequence). This holds without any further high-level assumption: it is a consequence of the geometric identification conditions (Assumptions 1 and 2) already imposed for Theorem 1. \square

Proof of Theorem 4. Step 1: CLT for projection estimators. Lemma D.8 gives

$$\sqrt{n} \operatorname{vec}((\widehat{P}_C - P_C, \widehat{P}_F - P_F, \widehat{P}_S - P_S)) \Rightarrow N(0, \Omega_P).$$

Step 2: CLT for similarity scores. The score map $P_D \mapsto S_D = \|P_D\|_F^2 = \operatorname{tr}(P_D^2)$ is continuously Fréchet-differentiable with derivative $\dot{S}_D[H] = 2\operatorname{tr}(P_D H) = 2\langle P_D, H \rangle_F$. Applying the multivariate delta method to the score map $(P_C, P_F, P_S) \mapsto (S_C, S_F, S_S)$,

$$\sqrt{n}(\widehat{S} - S) \Rightarrow N(0, \Omega_S), \quad \Omega_S = J_S \Omega_P J_S',$$

where J_S is the block-diagonal matrix of score derivatives $\dot{S}_D[\cdot]$, $D \in \mathfrak{D}$. (Composing this with the $\Gamma \mapsto P_D$ derivative $\Pi_{T_D(\Gamma_0)}$ from Lemma D.7 via the chain rule recovers, in a single step, the expression $\dot{S}_{D,\Gamma_0}[H] = 2\langle P_D(\Gamma_0), \Pi_{T_D(\Gamma_0)}(H) \rangle_F$ of Corollary 1; the two-stage decomposition used here and the single-stage chain rule used there compute the same derivative.)

Step 3: CLT for the dependence profile. Applying Lemma D.9 to Step 2,

$$\sqrt{n}(\widehat{\omega} - \omega) \Rightarrow N(0, G_\omega \Omega_S G_\omega'),$$

where G_ω is the Jacobian of the normalization map π given in Lemma D.9. Setting $\Xi = G_\omega \Omega_S G_\omega' = J_\omega \Omega_\Gamma J_\omega'$ with $J_\omega = G_\omega J_S \mathcal{D}$ completes the proof. \square

C.3 Proofs of Results in Sections 6 and 7

This subsection contains the proofs of Propositions 2, 3, and 4, Theorems 5, 6, and 7, and Corollary 2.

Proof of Proposition 2. If

$$\max_{d \in \mathfrak{D}} |\widehat{\omega}_d - \omega_d| \leq \frac{\Delta_\omega}{2},$$

then

$$\widehat{\omega}_{d^*} \geq \omega_{d^*} - \frac{\Delta_\omega}{2}$$

and

$$\widehat{\omega}_d \leq \omega_d + \frac{\Delta_\omega}{2}, \quad d \neq d^*.$$

Since

$$\omega_{d^*} - \omega_d \geq \Delta_\omega,$$

it follows that

$$\widehat{\omega}_{d^*} > \widehat{\omega}_d, \quad d \neq d^*.$$

Hence

$$\widehat{d} = d^*.$$

Taking complements yields the result. □

Proof of Theorem 5. By Theorem 3,

$$\max_{d \in \mathfrak{D}} |\widehat{\omega}_d - \omega_d| = o_p(1).$$

Under Assumption 7,

$$\Delta_\omega = \omega_{d^*} - \max_{d \neq d^*} \omega_d > 0.$$

Therefore, with probability approaching one,

$$\widehat{\omega}_{d^*} > \widehat{\omega}_d, \quad d \neq d^*,$$

so that

$$\widehat{d} = d^*.$$

Hence

$$P(\widehat{d} = d^*) \rightarrow 1.$$

□

Proof of Theorem 6. Let

$$Z_n = \sqrt{n} (\widehat{\omega}_{d_1} - \widehat{\omega}_{d_2}).$$

By the multivariate central limit theorem,

$$Z_n = c + e' \sqrt{n} (\widehat{\omega} - \omega_n) + o_p(1),$$

where

$$e = e_{d_1} - e_{d_2}.$$

Therefore

$$Z_n \Rightarrow N(c, e' \Xi e).$$

Since

$$\widehat{d} = d_1$$

if and only if

$$Z_n > 0,$$

it follows that

$$P(\widehat{d} = d_1) \rightarrow \Phi\left(\frac{c}{\sqrt{e' \Xi e}}\right).$$

The limit belongs to $(0, 1)$.

□

Proof of Proposition 3. By Theorem 3,

$$\widehat{\omega}_d \xrightarrow{p} \omega_d, \quad d \in \mathfrak{D}.$$

Similarly, consistency of the projection-residual diagnostics implies

$$\widehat{\rho}_d \xrightarrow{p} \rho_d, \quad d \in \mathfrak{D}.$$

Since the maximum, minimum, and product mappings are continuous, the continuous mapping theorem yields

$$\widehat{\kappa} = (1 - \widehat{\rho}_{\min}) \widehat{\Delta}_\omega \xrightarrow{p} (1 - \rho_{\min,0}) \Delta_{\omega,0} = \kappa_0.$$

□

Proof of Proposition 4. By Theorem 5,

$$P(\widehat{d} = d^*) \rightarrow 1.$$

For every $\varepsilon > 0$,

$$P\left(\left|\widehat{V}^* - V_{d^*}\right| > \varepsilon\right) \leq P(\widehat{d} \neq d^*) + P\left(\left|\widehat{V}_{d^*} - V_{d^*}\right| > \varepsilon\right).$$

The first term converges to zero by dominant-geometry consistency, and the second by assumption. Therefore

$$\widehat{V}^* \xrightarrow{p} V_{d^*}.$$

□

Proof of Theorem 7. By Theorem 5,

$$P(\widehat{d} = d^*) \rightarrow 1.$$

On the event $\{\widehat{d} = d^*\}$,

$$\widehat{V}^* = \widehat{V}_{d^*}.$$

Hence, for every $\varepsilon > 0$,

$$P\left(\left|\widehat{V}^* - \widehat{V}_{d^*}\right| > \varepsilon\right) \leq P(\widehat{d} \neq d^*) \rightarrow 0.$$

Therefore,

$$\widehat{V}^* - \widehat{V}_{d^*} = o_p(1).$$

Since $\widehat{V}_{d^*} \xrightarrow{p} V_{d^*}$, it follows that

$$\widehat{V}^* \xrightarrow{p} V_{d^*}.$$

□

Proof of Corollary 2. Let

$$A_n = \{\widehat{d} = d^*\}.$$

By Theorem 5,

$$P(A_n) \rightarrow 1.$$

On the event A_n , we have

$$\tau_{n,\widehat{d}} = \tau_{n,d^*} \quad \text{and} \quad \widehat{V}^* = \widehat{V}_{\widehat{d}} = \widehat{V}_{d^*}.$$

Therefore, on A_n ,

$$T_n^* = \frac{\tau_{n,\widehat{d}}(\widehat{\theta}_n - \theta_0)}{\sqrt{\widehat{V}^*}} = \frac{\tau_{n,d^*}(\widehat{\theta}_n - \theta_0)}{\sqrt{\widehat{V}_{d^*}}} = T_n^{oracle}.$$

Hence, for every $\varepsilon > 0$,

$$P(|T_n^* - T_n^{oracle}| > \varepsilon) \leq P(A_n^c) = P(\widehat{d} \neq d^*) \rightarrow 0.$$

Thus,

$$T_n^* - T_n^{oracle} = o_p(1).$$

By assumption,

$$T_n^{oracle} \Rightarrow N(0, 1).$$

Therefore, by Slutsky's theorem,

$$T_n^* = T_n^{oracle} + o_p(1) \Rightarrow N(0, 1).$$

□

A Auxiliary results and proofs

D.1 Two-Geometry Local Indistinguishability and Identification Proofs

Proof of Lemma A.5. Cluster projection uniqueness. At a regular cluster point Σ_C (Section A.1), every entry $(\Sigma_C)_{ab} \neq 0$ for $(a, b) \in \mathcal{I}_C$. By continuity of matrix entries, any Σ within a sufficiently small $\|\cdot\|_F$ -ball around Σ_C satisfies $\Sigma_{ab} \neq 0$ for $(a, b) \in \mathcal{I}_C$, so the active support pattern is locally constant at \mathcal{I}_C . The cluster projection $P_C(\Sigma) = M_C \odot \Sigma$ is the orthogonal projection onto the linear subspace $\mathcal{V}_{\mathcal{I}_C}$, which is unique.

Sparse projection uniqueness. The same argument applies verbatim with \mathcal{I}_C replaced by \mathcal{I}_S : Assumption 2 ensures the active support pattern is locally stable, so $P_S(\Sigma) = \text{projection onto } \mathcal{V}_{\mathcal{I}_S}$ is locally unique.

Factor projection uniqueness. Write $\Sigma_F = L_0 + D_0$ with L_0 of rank r and r distinct positive leading eigenvalues, as in the regularity condition of Section A.1. We establish *local* uniqueness of the projection in a neighborhood of Σ_F ; global uniqueness of the minimizer of the (nonconvex) factor objective is not claimed.

Fix D in a neighborhood of D_0 and consider the rank- r truncation of $\Sigma_F - D$. By Weyl’s inequality, the eigenvalues of $\Sigma_F - D$ depend continuously on D , so for D sufficiently close to D_0 the r leading eigenvalues of $\Sigma_F - D$ remain positive and distinct (by the regularity assumption on $L_0 = \Sigma_F - D_0$). Under this condition, the Eckart–Young theorem implies that the best rank- r approximation $L^*(D) = \arg \min_{\text{rank}(L) \leq r} \|(\Sigma_F - D) - L\|_F$ is the unique truncated eigendecomposition of $\Sigma_F - D$, and the map $D \mapsto L^*(D)$ is continuous (indeed, real-analytic away from eigenvalue crossings; see Lewis and Malick, 2008, Section 3). Composing with the diagonal-update step, the fixed-point equation $D = \text{diag}(\Sigma_F - L^*(D))$ defines a continuous self-map on a compact neighborhood of D_0 . At D_0 this map is satisfied by construction, and its derivative is a contraction in a neighborhood of D_0 because the derivative of $L^*(\cdot)$ with respect to D is controlled by the eigengap implied by the regularity condition (the relevant first-order perturbation bound for L^* is the matrix Davis–Kahan bound, which is Lipschitz in D with constant inversely proportional to the eigengap of L_0). Consequently the fixed point D^* is locally unique near D_0 , and so is $L^* = L^*(D^*)$. The projection $P_F(\Sigma_F) = L^* + D^*$ is therefore locally unique in a neighborhood of Σ_F .

This establishes local, not global, uniqueness of P_F : the factor projection objective is nonconvex in (L, D) jointly, and the argument above does not rule out the existence of other, non-nearby stationary points of the same objective away from Σ_F . Local identification of the dependence profile (Theorem 1) only requires local uniqueness, so this suffices for the stated result; it does not establish that the alternating-projection algorithm of Section B.1 converges to the population projection $P_F(\Sigma)$ from an arbitrary initialization when Σ is far from a regular point. \square

D.2 Technical results

We first record the elementary fact, specific to the finite-dimensional setting of this paper, that reduces Hadamard differentiability to the easier-to-verify property of directional differentiability with a linear derivative.

Lemma D.6 (Directional Differentiability with Linear Derivative Implies Hadamard Differ-

entiability in Finite Dimensions). Let $f : \mathbb{H} \rightarrow \mathbb{H}$ with \mathbb{H} finite-dimensional. Suppose f is directionally differentiable at Σ_0 with derivative map $H \mapsto Df(\Sigma_0)[H]$ that is linear in H . Then f is Hadamard differentiable at Σ_0 with the same derivative.

Proof. Let $t_m \downarrow 0$ and $H_m \rightarrow H$ in \mathbb{H} . We must show

$$\frac{f(\Sigma_0 + t_m H_m) - f(\Sigma_0)}{t_m} \rightarrow Df(\Sigma_0)[H].$$

Write

$$\begin{aligned} \frac{f(\Sigma_0 + t_m H_m) - f(\Sigma_0)}{t_m} - Df(\Sigma_0)[H] &= \underbrace{\left(\frac{f(\Sigma_0 + t_m H_m) - f(\Sigma_0)}{t_m} - Df(\Sigma_0)[H_m] \right)}_{\text{(I)}} \\ &\quad + \underbrace{(Df(\Sigma_0)[H_m] - Df(\Sigma_0)[H])}_{\text{(II)}}. \end{aligned}$$

Term (II) vanishes as $m \rightarrow \infty$ because $Df(\Sigma_0)[\cdot]$ is linear, hence continuous, on the finite-dimensional space \mathbb{H} , and $H_m \rightarrow H$. For term (I), fix $\varepsilon > 0$. Since $H_m \rightarrow H$, the sequence $\{H_m\}$ is contained in a compact set $K \subset \mathbb{H}$ (e.g. a closed ball containing all H_m and H). Directional differentiability at Σ_0 means that for every fixed direction $H' \in \mathbb{H}$,

$$\frac{f(\Sigma_0 + tH') - f(\Sigma_0)}{t} \rightarrow Df(\Sigma_0)[H'] \quad \text{as } t \downarrow 0.$$

Because \mathbb{H} is finite-dimensional, f is continuous near Σ_0 (by Lemma D.13, $f = P_D$ is locally Lipschitz), and the convergence in the displayed directional limit is, in fact, locally uniform over H' ranging over the compact set K : this is because the difference quotient (I), viewed as a function of $(t, H') \in (0, 1] \times K$, extends continuously to $t = 0$ with value 0 at every $H' \in K$ (directional differentiability), and a continuous function on the compact set $\{0\} \times K$ that is identically zero is, by continuity on the compact set $[0, 1] \times K$ for t near 0, uniformly close to zero for t small, uniformly in $H' \in K$. This is the standard finite-dimensional fact that pointwise convergence of a locally equicontinuous (here, Lipschitz with a common local constant, by Lemma D.13) family of difference quotients on a compact set is uniform. Hence for m and t_m small enough, $\|(I)\|_F < \varepsilon$. Combining the two terms gives the result. \square

Lemma D.7 (Hadamard Differentiability of Projection Maps). *At regular points satisfying local prox-regularity and local uniqueness, P_D is Hadamard differentiable, with derivative given by orthogonal projection onto the tangent space $T_D(\Sigma_0)$:*

$$DP_D(\Sigma_0)[H] = \Pi_{T_D(\Sigma_0)}(H), \quad H \in \mathbb{H},$$

where $\Pi_{T_D(\Sigma_0)}$ denotes the orthogonal projection (in the Frobenius inner product) onto $T_D(\Sigma_0)$.

Proof of Lemma D.7. By Lemma D.6, it suffices to show that P_D is directionally differentiable at the relevant regular point with a linear derivative equal to $\Pi_{T_D(\Sigma_0)}$.

Cluster and sparse geometries. At a regular cluster (respectively, sparse) point Σ_0 , the active support \mathcal{I}_D is locally constant by the argument in the proof of Lemma A.5: there is a neighborhood of Σ_0 on which $P_D(\Sigma) = M_D \odot \Sigma$ for the *same* fixed support mask M_D . Thus, on this neighborhood, P_D coincides with the fixed linear map $\Sigma \mapsto M_D \odot \Sigma$, which is exactly the orthogonal projection onto $T_D(\Sigma_0) = \mathcal{V}_{\mathcal{I}_D}$ (linearity of the Hadamard product in its second argument, together with $T_D(\Sigma_0) = \mathcal{V}_{\mathcal{I}_D}$ from Section A.1). A map that is linear in a neighborhood of Σ_0 is trivially directionally differentiable there with derivative equal to the map itself, i.e. $DP_D(\Sigma_0)[H] = M_D \odot H = \Pi_{T_D(\Sigma_0)}(H)$, which is linear in H .

Factor geometry. At a regular factor point $\Sigma_0 = \Sigma_F$, the proof of Lemma A.5 shows that P_F is locally single-valued and, by Lemma D.13, locally Lipschitz, via the local correspondence with the smooth fixed-rank manifold \mathcal{M}_r of Lewis and Malick (2008). Because Σ_F has r distinct positive leading eigenvalues, \mathcal{M}_r is a C^2 embedded submanifold of \mathbb{H} in a neighborhood of Σ_F , with tangent space at Σ_F equal to $T_F(\Sigma_F)$ as given in Section A.1 (this is the standard tangent-space characterization of the fixed-rank PSD-plus-diagonal manifold; see Lewis and Malick, 2008, Section 2). For the Euclidean metric projection onto a C^2 submanifold, directional differentiability at a point where the projection is single-valued is a classical fact of Riemannian/matrix sensitivity analysis: writing $P_F(\Sigma_F + tH)$ for small t and expanding the first-order optimality condition that $\Sigma_F + tH - P_F(\Sigma_F + tH)$ is orthogonal to the tangent space of \mathcal{M}_r at $P_F(\Sigma_F + tH)$, a Taylor expansion in t (using smoothness of the manifold and continuity of P_F near Σ_F , both available here) gives

$$\frac{P_F(\Sigma_F + tH) - P_F(\Sigma_F)}{t} \rightarrow \Pi_{T_F(\Sigma_F)}(H) \quad \text{as } t \downarrow 0,$$

because at $\Sigma_F \in \mathcal{M}_r$ the residual $\Sigma_F - P_F(\Sigma_F) = D_F$ is itself orthogonal to $T_F(\Sigma_F)$ under the regularity condition (the noise floor is orthogonal to the rank- r tangent directions and to the diagonal perturbations already spanned by $T_F(\Sigma_F)$), so the first-order correction in the projection is exactly the tangential component of H , with no contribution from the curvature of \mathcal{M}_r entering at first order. This derivative, $H \mapsto \Pi_{T_F(\Sigma_F)}(H)$, is linear in H , since $T_F(\Sigma_F)$ is a fixed linear subspace once Σ_F is fixed.

In all three cases the directional derivative is linear in H , so Lemma D.6 applies and gives Hadamard differentiability with $DP_D(\Sigma_0)[H] = \Pi_{T_D(\Sigma_0)}(H)$. \square

Lemma D.8 (Joint CLT for Projection Estimators). *Under Assumption 5,*

$$\sqrt{n} \begin{pmatrix} \text{vec}(\widehat{P}_C - P_C) \\ \text{vec}(\widehat{P}_F - P_F) \\ \text{vec}(\widehat{P}_S - P_S) \end{pmatrix} \Rightarrow N(0, \Omega_P).$$

Proof. By Lemma D.7, each P_C, P_F, P_S is Hadamard differentiable at Γ_0 (a regular point of each geometry, by Assumptions 1 and 2), with derivative $DP_D(\Gamma_0)[H] = \Pi_{T_D(\Gamma_0)}(H)$, $D \in \{C, F, S\}$. Hadamard differentiability of each coordinate map implies Hadamard differentiability of the product map

$$\Gamma \mapsto (P_C(\Gamma), P_F(\Gamma), P_S(\Gamma))$$

at Γ_0 , with derivative $\mathcal{D}[H] = (\Pi_{T_C(\Gamma_0)}(H), \Pi_{T_F(\Gamma_0)}(H), \Pi_{T_S(\Gamma_0)}(H))$, since Hadamard differentiability is preserved under finite Cartesian products of differentiable maps (apply the definition coordinatewise to the same sequence $t_m \downarrow 0, H_m \rightarrow H$). By Assumption 5, $\sqrt{n} \text{vec}(\widehat{\Gamma}_n - \Gamma_0) \Rightarrow N(0, \Omega_\Gamma)$ (as a special case of the asymptotic linear representation with $\Omega_\Gamma = E(\psi_i \psi_i')$). The functional delta method (van der Vaart and Wellner, 1996, Theorem 3.9.4) applied to this product map then gives

$$\sqrt{n} \begin{pmatrix} \text{vec}(\widehat{P}_C - P_C) \\ \text{vec}(\widehat{P}_F - P_F) \\ \text{vec}(\widehat{P}_S - P_S) \end{pmatrix} \Rightarrow N(0, \Omega_P), \quad \Omega_P = \mathcal{D} \Omega_\Gamma \mathcal{D}',$$

where \mathcal{D} is the matrix representation of the linear map $H \mapsto (\Pi_{T_C(\Gamma_0)}(H), \Pi_{T_F(\Gamma_0)}(H), \Pi_{T_S(\Gamma_0)}(H))$ acting on $\text{vec}(H)$. \square

Lemma D.9 (Delta Method for Dependence Profiles). *Let $S = (S_C, S_F, S_S)'$ and $S_T > 0$. Then*

$$\sqrt{n}(\widehat{\omega} - \omega) = G_\omega \sqrt{n}(\widehat{S} - S) + o_p(1),$$

where

$$G_\omega = \frac{1}{S_T^2} \begin{pmatrix} S_F + S_S & -S_C & -S_C \\ -S_F & S_C + S_S & -S_F \\ -S_S & -S_S & S_C + S_F \end{pmatrix}.$$

Proof. The map $g(S) = S/S_T$ is continuously differentiable when $S_T > 0$. The displayed matrix is its Jacobian. The result follows from the multivariate delta method. \square

Proposition D.5 (Operator Invariance). *Suppose two population dependence operators Γ_1 and Γ_2 satisfy*

$$\Gamma_2 = a\Gamma_1, \quad a > 0.$$

Assume that each covariance geometry \mathcal{S}_d , $d \in \mathfrak{D}$, is a cone. Then

$$\omega_d(\Gamma_1) = \omega_d(\Gamma_2), \quad d \in \mathfrak{D}.$$

Proof of Proposition D.5. Fix $D \in \{C, F, S\}$. Each geometry is a cone: \mathcal{S}_C and \mathcal{S}_S are cones because their support constraints are homogeneous; $\mathcal{S}_F(r)$ is a cone by Lemma D.12. By definition,

$$P_D(\Gamma_1) = \arg \min_{\Gamma \in \mathcal{S}_D} \|\Gamma_1 - \Gamma\|_F.$$

Let $\Gamma_2 = a\Gamma_1$ for $a > 0$. Since \mathcal{S}_D is a cone,

$$\Gamma \in \mathcal{S}_D \iff a^{-1}\Gamma \in \mathcal{S}_D.$$

Therefore,

$$P_D(\Gamma_2) = \arg \min_{\Gamma \in \mathcal{S}_D} \|a\Gamma_1 - \Gamma\|_F.$$

Using the change of variables

$$\Gamma = a\tilde{\Gamma}, \quad \tilde{\Gamma} \in \mathcal{S}_D,$$

we obtain

$$P_D(\Gamma_2) = a \arg \min_{\tilde{\Gamma} \in \mathcal{S}_D} \|\Gamma_1 - \tilde{\Gamma}\|_F.$$

Hence

$$P_D(\Gamma_2) = aP_D(\Gamma_1).$$

It follows that the similarity score satisfies

$$S_D(\Gamma_2) = \|P_D(\Gamma_2)\|_F^2 = \|aP_D(\Gamma_1)\|_F^2 = a^2\|P_D(\Gamma_1)\|_F^2 = a^2S_D(\Gamma_1).$$

Similarly,

$$S_T(\Gamma_2) = \sum_{D \in \{C, F, S\}} S_D(\Gamma_2) = a^2 \sum_{D \in \{C, F, S\}} S_D(\Gamma_1) = a^2 S_T(\Gamma_1).$$

Therefore,

$$\omega_D(\Gamma_2) = \frac{S_D(\Gamma_2)}{S_T(\Gamma_2)} = \frac{a^2 S_D(\Gamma_1)}{a^2 S_T(\Gamma_1)} = \frac{S_D(\Gamma_1)}{S_T(\Gamma_1)} = \omega_D(\Gamma_1).$$

Since this holds for every $D \in \{C, F, S\}$, the dependence profile is invariant to positive scalar rescaling of the dependence operator. □

D.3 Geometry of Covariance Classes

Lemma D.10 (Closedness of the Generalized Cluster Geometry). *Fix n and let \mathfrak{I}_C denote the family of all admissible cluster-support sets generated by one-way, two-way, or multiway clustering structures on $\{1, \dots, n\}$. For each $\mathcal{I} \in \mathfrak{I}_C$, define*

$$\mathcal{V}_{\mathcal{I}} = \{\Gamma \in \mathbb{H} : \Gamma_{ij} = 0 \text{ whenever } (i, j) \notin \mathcal{I}\}.$$

Define the generalized cluster class by

$$\mathcal{S}_C = \bigcup_{\mathcal{I} \in \mathfrak{I}_C} \mathcal{V}_{\mathcal{I}}.$$

Then \mathcal{S}_C is closed in \mathbb{H} . Moreover, each $\mathcal{V}_{\mathcal{I}}$ is a closed linear subspace of \mathbb{H} .

Proof. Fix n and the maximum number of clustering dimensions M (treated as fixed throughout the paper). The number of admissible support patterns \mathfrak{I}_C is finite: each clustering dimension partitions $\{1, \dots, n\}$ into at most n groups, and a one-way support pattern is determined by a single such partition, so the total number of patterns is bounded by the M -fold product of the number of set partitions of $\{1, \dots, n\}$, which is finite for fixed n and M . Each $\mathcal{V}_{\mathcal{I}}$ is a closed linear subspace because it is defined by linear equality constraints ($\Gamma_{ab} = 0$ for $(a, b) \notin \mathcal{I}$). A finite union of closed sets is closed. Therefore \mathcal{S}_C is closed. □

Lemma D.11 (Closedness of Sparse Geometry). *For fixed n ,*

$$\mathcal{S}_S = \{\Gamma : |\text{supp}(\Gamma)| \leq k_n\}$$

is closed in \mathbb{H} .

Proof. For each index set I , let

$$\mathcal{V}_I = \{\Gamma : \Gamma_{ij} = 0 \text{ for } (i, j) \notin I\}.$$

Each \mathcal{V}_I is a closed linear subspace. Since

$$\mathcal{S}_S = \bigcup_{|I| \leq k_n} \mathcal{V}_I$$

and the union is finite for fixed n , \mathcal{S}_S is closed. \square

Lemma D.12 (Closedness and Cone Property of the Factor Geometry). *For fixed r , $\mathcal{S}_F(r)$ is closed in \mathbb{H} . Moreover, $\mathcal{S}_F(r)$ is a cone: for every $\Gamma \in \mathcal{S}_F(r)$ and $a > 0$, $a\Gamma \in \mathcal{S}_F(r)$.*

Proof. Closedness. Let $\Gamma_m = L_m + D_m \in \mathcal{S}_F(r)$ with $\Gamma_m \rightarrow \Gamma$ in $\|\cdot\|_F$. The diagonal map $\Gamma \mapsto \text{diag}(\Gamma)$ is continuous, so $D_m = \text{diag}(\Gamma_m) \rightarrow D = \text{diag}(\Gamma)$. Hence $L_m = \Gamma_m - D_m \rightarrow L = \Gamma - D$. Since $\{\Gamma : \text{rank}(\Gamma) \leq r\}$ is closed (as a finite union of algebraic varieties), $\text{rank}(L) \leq r$. Also $\Gamma \succeq 0$ as a limit of PSD matrices. Thus $\Gamma = L + D \in \mathcal{S}_F(r)$.

Cone property. If $\Gamma = L + D \in \mathcal{S}_F(r)$ and $a > 0$, then $a\Gamma = aL + aD$ where $\text{rank}(aL) = \text{rank}(L) \leq r$ and aD is diagonal with non-negative entries. Hence $a\Gamma \in \mathcal{S}_F(r)$. \square

D.4 Projection Regularity

Lemma D.13 (Prox-regularity and Local Lipschitz Continuity of Projections). *At regular points, each covariance geometry \mathcal{S}_D is locally prox-regular. Consequently, P_D is locally single-valued and Lipschitz: for Σ_1, Σ_2 sufficiently close to a regular point Σ_0 ,*

$$\|P_D(\Sigma_1) - P_D(\Sigma_2)\|_F \leq L_D \|\Sigma_1 - \Sigma_2\|_F.$$

Proof. We verify prox-regularity for each geometry; the Lipschitz conclusion then follows from Rockafellar and Wets (1998), Theorem 13.37.

Cluster geometry. At a regular cluster point, \mathcal{S}_C coincides locally with the linear subspace $\mathcal{V}_{\mathcal{I}_C}$. Linear subspaces are convex, hence prox-regular with any radius $r > 0$.

Sparse geometry. At a regular sparse point, \mathcal{S}_S coincides locally with $\mathcal{V}_{\mathcal{I}_S}$, which is again a linear subspace. The same argument applies.

Factor geometry. The set $\mathcal{S}_F(r)$ contains the fixed-rank stratum $\mathcal{M}_r = \{L + D : \text{rank}(L) = r, D \text{ diagonal}, L + D \succeq 0\}$. By Lewis and Malick (2008), Theorem 1, the fixed-rank manifold is prox-regular at matrices with r distinct positive singular values, which holds at regular factor points by assumption. Prox-regularity is itself a local, pointwise property and is unaffected by the global nonconvexity of $\mathcal{S}_F(r)$ noted in the proof of Lemma A.5: it guarantees that P_F is single-valued and Lipschitz in a neighborhood of a regular point, without requiring or implying that the factor projection is globally unique on all of $\mathcal{S}_F(r)$. \square

A Simulation Design

Section 8 of the main paper reports the benchmark Monte Carlo evidence on three questions: recovery of the dominant covariance geometry, classification under hybrid and near-tie dependence, and the performance of profile-guided inference relative to the infeasible oracle. This appendix provides the implementation details underlying those results: the baseline data-generating processes, parameter calibrations, the empirical dependence operator, and the projection algorithms. It also reports supplementary robustness checks on principal-angle separation, operator misspecification, and oracle tracking. Table E.1 summarizes the baseline designs.

Table E.1: Summary of Simulation Designs

Design	Dominant Geometry	Purpose
Cluster	Cluster	Benchmark structured-support dependence
Factor	Factor	Benchmark low-rank dependence
Sparse	Sparse / none-of-the-above	Network-generated dependence
Hybrid	Mixed	Coexistence of multiple geometries
Near tie	Ambiguous	Local alternatives and classification uncertainty
Oracle sweep	Varies	Profile-guided inference versus oracle benchmark

Throughout, the main reported objects are the estimated dependence profile $\widehat{\omega} = (\widehat{\omega}_C, \widehat{\omega}_F, \widehat{\omega}_S)'$ and the projection-residual diagnostics $\widehat{\rho}_C, \widehat{\rho}_F, \widehat{\rho}_S, \widehat{\rho}_{\min} = \min_{d \in \mathfrak{D}} \widehat{\rho}_d$. Consistent with the main paper, the goal of this section is to assess how well these statistics recover the covariance geometry encoded in the chosen empirical dependence operator, rather than to compare variance estimators by coverage or mean squared error.

E.1 Baseline Regression Model and Empirical Operator

For each replication, we generate

$$y_{it} = x_i' \beta + u_{it}, \quad i = 1, \dots, n, \quad t = 1, \dots, T, \quad (\text{E.1})$$

with $x_i = (1, x_{i1}, x_{i2})'$, $x_{i1}, x_{i2} \stackrel{iid}{\sim} N(0, 1)$, and $\beta = (1, 1, 1)'$. The dependence structure varies through $u_t = (u_{1t}, \dots, u_{nt})'$ across the designs described below. In each replication, we estimate β by OLS period by period and use the averaged residual covariance operator

$$\widehat{\Gamma}_n = \frac{1}{T} \sum_{t=1}^T \widehat{u}_t \widehat{u}_t'$$

as the baseline empirical dependence operator. Averaging over $T = 50$ periods avoids the rank-one degeneracy of a single outer-product operator and allows the cluster, factor, and sparse projection scores to vary meaningfully across designs.

E.2 Population Dependence Designs

Design 1: Pure Cluster. Partition observations into G clusters $\mathcal{C} = \{C_1, \dots, C_G\}$ and set $u_i = a_{g(i)} + \varepsilon_i$ with $a_g \sim N(0, \sigma_a^2)$, $\varepsilon_i \sim N(0, \sigma_\varepsilon^2)$ independent across g and i , giving $\Sigma_C = \sigma_a^2 Z Z' + \sigma_\varepsilon^2 I_n$, where Z is the $n \times G$ cluster-membership matrix.

Design 1B: Two-Way Cluster. For observations indexed by (i, t) , $i = 1, \dots, N$, $t = 1, \dots, T$, set $u_{it} = a_i + b_t + \varepsilon_{it}$ with $a_i \sim N(0, \sigma_a^2)$, $b_t \sim N(0, \sigma_b^2)$, $\varepsilon_{it} \sim N(0, \sigma_\varepsilon^2)$ independent. Unlike one-way clustering, the resulting covariance matrix is not block diagonal, so the design also carries non-negligible sparse affinity.

Design 2: Pure Factor. Set $u_i = \lambda_i f + \varepsilon_i$ with $f \sim N(0, \sigma_f^2)$, $\lambda_i \sim N(0, \sigma_\lambda^2)$ i.i.d., giving $\Sigma_F = \sigma_f^2 \lambda \lambda' + \sigma_\varepsilon^2 I_n$. Baseline values are $\sigma_f^2 = 1$, $\sigma_\lambda = 1$. Loadings λ are drawn once with a fixed seed and held constant across replications (fixed-design setting); multi-factor versions with $f \in \mathbb{R}^r$, $r \in \{1, 2, 3\}$, are also considered.

Remark E.1 (Mean-Zero Loadings and the Fixed-Design Realization). *The mean-zero specification follows the econometric factor-model literature (Bai and Ng, 2002; Bai, 2003) and matters mechanically here: because regression (E.1) includes a constant, OLS residuals lie in the orthogonal complement of $\text{col}(X)$, and if λ were nearly proportional to $\mathbf{1}_n$, OLS would remove most of the factor signal from the residuals. Since the simulation fixes λ at a single draw across all replications, what matters in practice is the realized sample mean $\bar{\lambda} = n^{-1} \sum_i \lambda_i$ for that draw, not the population mean $E[\lambda_i] = 0$ alone. For the fixed seed used throughout (seed 9901), $\bar{\lambda} = -0.0407$ (standardized magnitude $\bar{\lambda} \sqrt{n} = -0.644$), confirming that λ is close to orthogonal to $\mathbf{1}_n$ for this realization and that OLS retains the bulk of the factor signal.*

Design 3: Pure Sparse. Let W be an $n \times n$ sparse adjacency matrix (Erdős–Rényi with $P(W_{ij} = 1) = c/n$, or q -nearest-neighbor on random locations in $[0, 1]^2$). Disturbances follow the spatial autoregression $u = (I_n - \rho W)^{-1} \varepsilon$, $\varepsilon \sim N(0, \sigma_\varepsilon^2 I_n)$, with ρ chosen so $I_n - \rho W$ is nonsingular.

Designs 4–5: Hybrids. Cluster–factor hybrids set $u_i = \alpha_C a_{g(i)} + \alpha_F \lambda_i f + \varepsilon_i$ with $(\alpha_C, \alpha_F) \in \{(1, 0), (0.75, 0.25), (0.5, 0.5), (0.25, 0.75), (0, 1)\}$, implying $\Sigma = \alpha_C^2 \sigma_a^2 Z Z' + \alpha_F^2 \sigma_f^2 \lambda \lambda' + \sigma_\varepsilon^2 I_n$. The most general design adds a sparse component, $u = \alpha_C Z a + \alpha_F \Lambda f + \alpha_S (I_n - \rho W)^{-1} \varepsilon + \eta$ with $\eta \sim N(0, \sigma_\eta^2 I_n)$, and is evaluated at

$$(\alpha_C, \alpha_F, \alpha_S) \in \left\{ (1, 0, 0), (0, 1, 0), (0, 0, 1), (1, 1, 0), (1, 0, 1), (0, 1, 1), (1, 1, 1) \right\}.$$

E.3 Projection Implementation and Performance Measures

Given an empirical dependence operator $\widehat{\Gamma}$: the *cluster* projection is $\widehat{P}_C = M_C \odot \widehat{\Gamma}$ for the known cluster-support matrix M_C (Section 2); the *factor* projection $\widehat{P}_F = L^* + D^*$ is computed by the alternating-projection algorithm of Section B.1 applied to $\widehat{\Gamma}_n$, with rank r set to the true number of factors at baseline ($r \in \{1, 2, 3\}$ as a robustness check); the *sparse* projection \widehat{P}_S retains the k_n largest off-diagonal entries of $\widehat{\Gamma}$ in absolute value and zeroes the rest, keeping all diagonal entries.

For each $D \in \mathfrak{D} = \{C, F, S\}$, compute $\widehat{S}_D = \|\widehat{P}_D\|_F^2$, $\widehat{\omega}_D = \widehat{S}_D / \sum_{D'} \widehat{S}_{D'}$, and $\widehat{\rho}_D = \|\widehat{\Gamma} - \widehat{P}_D\|_F / \|\widehat{\Gamma}\|_F$, with $\widehat{\rho}_{\min} = \min_D \widehat{\rho}_D$. We report Monte Carlo means, standard deviations, and $\text{RMSE}_\omega = [E\{\|\widehat{\omega} - \omega\|^2\}]^{1/2}$ relative to the population profile ω , together with the population procedure confidence index $\kappa_0 = (1 - \rho_{\min,0}) \Delta_{\omega,0}$, where $\rho_{\min,0}$ is the population minimum residual and $\Delta_{\omega,0} = \omega_{d^*} - \max_{d \neq d^*} \omega_d$ is the population separation margin. Large κ_0 signals a design in which one geometry clearly dominates *and* the covariance dictionary fits well in an absolute sense, so the procedure recommendation of Section 7.3 should be reliable; small κ_0 warns that the recommendation should be interpreted cautiously, whether because of near-tie separation or poor dictionary fit.

E.4 Near-Ties: Construction

Table 2 and Figure 2 in the main paper illustrate Theorem 6’s prediction that classification remains probabilistic under local separation. The underlying design is

$$u_i = \alpha_n \sigma_a a_{g(i)} + (1 - \alpha_n) \lambda_i f + \varepsilon_i, \quad \alpha_n = \frac{1}{2} + \frac{c}{\sqrt{n}},$$

with $\sigma_a^2 = \|\lambda \lambda'\|_F / \|Z Z'\|_F \approx 5.49$ chosen so the cluster and factor signal components have equal Frobenius norm, ensuring that c controls the cluster–factor *balance* rather than their relative scale. The implied population covariance is

$$\Sigma(\alpha_n) = \alpha_n^2 \sigma_a^2 Z Z' + (1 - \alpha_n)^2 \lambda \lambda' + \sigma_\varepsilon^2 I_n. \quad (\text{E.2})$$

Remark E.2 (Signal Scaling Versus Norm Normalization). *Dividing both signal matrices by their own Frobenius norms before mixing is an alternative route to scale balance, but it reduces all off-diagonal entries to $O(n^{-1})$, destroying the geometric signal relative to the noise floor $\sigma_\varepsilon^2 I_n$. Scaling by σ_a instead preserves the natural magnitude of off-diagonal entries and lets the procedure distinguish cluster from factor dependence at moderate sample sizes.*

Figure E.1 plots the full classification-frequency profile underlying Table 2—the Monte Carlo frequency with which the classifier selects each geometry as c varies—complementing the margin-versus-error view of Figure 2 in the main paper.

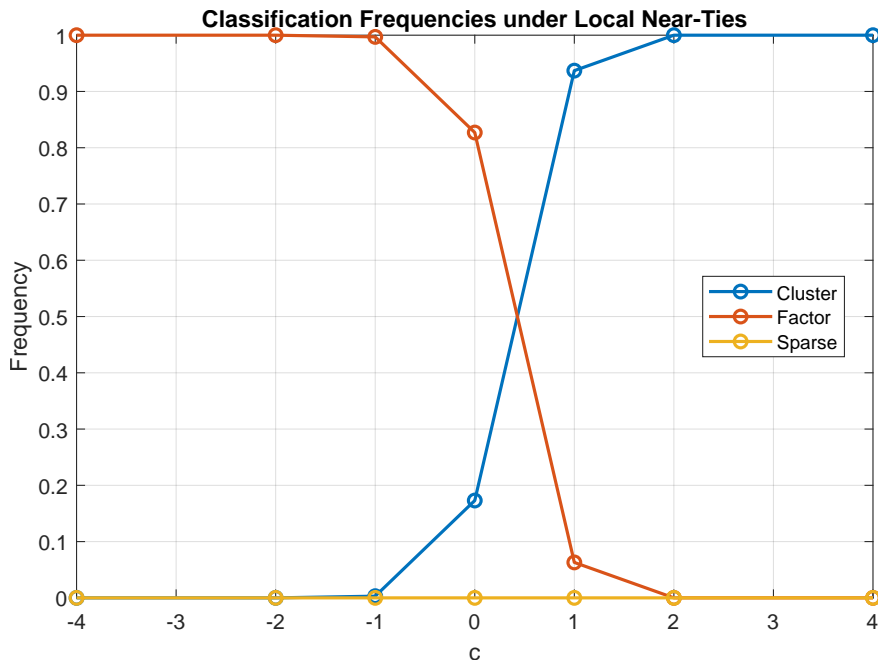


Figure E.1: Classification Frequencies under Local Near-Ties, by Geometry
Notes: Monte Carlo frequency with which the classifier selects each geometry as c varies, underlying the columns of Table 2.

The asymmetric separation margin visible in Table 2 around $c = 0$ (e.g., $\Delta_\omega = 0.312$ at $c = -1$ versus 0.145 at $c = +1$) reflects the cluster–sparse tangent-space overlap documented in Table E.2 below: when $c > 0$ (cluster-leaning), the sparse projection’s $k_n = 625$ largest off-diagonal entries fall disproportionately inside the cluster support, inflating ω_S at the expense of the cluster–factor gap, whereas the factor signal spreads comparable-magnitude entries across all $\binom{n}{2}$ pairs and receives no such boost when $c < 0$. This is a structural feature of the sparse projection’s geometry, not a violation of Proposition 2, which bounds misclassification by both the margin *and* the sampling variability of $\hat{\omega}$ —the latter is also smaller on the $c > 0$ side here, so a smaller margin at $c = +1$ remains consistent with the high classification frequency reported in the main text.

E.5 Simulation Parameters

The baseline design uses $n = 250$, $T = 50$, $B = 1,000$ Monte Carlo replications. Robustness checks vary $n \in \{100, 250, 500\}$, $T \in \{25, 50, 100\}$, the number of clusters $G \in \{10, 25, 50\}$ (balanced, $G = 25$ at baseline), factor strength $\sigma_f^2 \in \{0.25, 1, 4\}$ (baseline 1, with $\sigma_\varepsilon = 0.5$ throughout), and sparse network average degree $c \in \{2, 5, 10\}$ (baseline 5). The sparse projection’s sparsity level is $k_n = \lfloor 0.01n^2 \rfloor = 625$, well below the one-way cluster support ($G \cdot (n/G)^2 = 2,500$ entries at baseline), so that cluster and sparse geometries remain geometrically distinguishable by construction. For the near-tie design (Section E.4), $\sigma_a^2 \approx 5.49$, $\sigma_a \approx 2.34$, calibrated as described above.

E.6 Principal-Angle Diagnostics

Assumption 1 (positive off-diagonal principal angles) is a hypothesis of Theorems 1, 3, and 4. We check it directly at the population covariance matrices used in the baseline designs, computing the off-diagonal principal angle $\theta(T_D^{\text{off}}, T_{D'}^{\text{off}})$ between each pair of geometries (construction in Section A.1).

Table E.2: Principal-Angle Diagnostics

Design	$\theta(T_C^{\text{off}}, T_F^{\text{off}})$	$\theta(T_C^{\text{off}}, T_S^{\text{off}})$	$\theta(T_F^{\text{off}}, T_S^{\text{off}})$
Cluster (pure)	64.7°	0.0°	64.8°
Factor (pure)	64.7°	0.0°	20.4°
Sparse (pure)	64.7°	0.0°	66.0°
Cluster–Sparse	64.7°	0.0°	72.2°
Factor–Sparse	64.7°	0.0°	20.4°

Notes: The table reports the smallest off-diagonal principal angle $\theta(T_D^{\text{off}}, T_{D'}^{\text{off}})$ between each pair of covariance geometries, computed at the population covariance matrix of each baseline design. A value of 0° indicates the off-diagonal tangent spaces overlap at that design, so Assumption 1 fails for that pair there. The cluster–factor angle does not depend on the sparse design and is reported once, since T_C^{off} and T_F^{off} depend only on the cluster partition and factor loading, not the sparse component.

Two findings stand out. First, $\theta(T_C^{\text{off}}, T_S^{\text{off}}) = 0^\circ$ at every design: the sparse projection’s support (the $k_n = 625$ largest off-diagonal entries) is partly or, for the Cluster–Sparse design, entirely contained within the cluster support, so Assumption 1 is *not* satisfied for the cluster–sparse pair at these parameters. Second, $\theta(T_C^{\text{off}}, T_F^{\text{off}}) \approx 69^\circ$ across all designs, confirming the cluster–factor pair is well separated along off-diagonal directions at the realized factor loading, consistent with Remark A.1. The factor–sparse angle is more variable across independent draws of the sparse network (informally, resampling W across many seeds with λ fixed typically gives 65° – 72° for the pure Sparse design, though any single realization can

fall outside that range, as it does here).

These findings qualify, rather than undermine, the main results: the local-identification guarantee of Theorem 1 does not, strictly, apply to the cluster–sparse pair at these parameters, yet the estimated profile and classifier continue to behave sensibly (the Cluster–Sparse design’s separation margin $\Delta_{\omega,0} = 0.193$ remains comfortably bounded away from zero despite the principal-angle violation). This is consistent with Assumption 1 being sufficient, not necessary, for usable classification: Theorem 5 relies on Assumption 7 (separation of the ω_d themselves), which can hold even when the principal-angle condition does not.

E.7 Projection-Residual Diagnostics: Out-of-Dictionary Components

To probe the absolute-fit role of $\hat{\rho}_{\min}$ described in Section 4.2, we consider $\Gamma = \Gamma_C + \Gamma_F + \Gamma_S + \Gamma_R$, where $\Gamma_R = \tau BB'/n$ is a dense out-of-dictionary component, B an $n \times n$ matrix of independent standard normal entries, and $\tau \geq 0$ controls its magnitude.

Table E.3: Projection-Residual Diagnostics

τ	$\hat{\rho}_C$	$\hat{\rho}_F$	$\hat{\rho}_S$	$\hat{\rho}_{\min}$
$\tau = 0.00$	0.949	0.281	0.806	0.281
$\tau = 0.25$	0.947	0.304	0.806	0.304
$\tau = 0.50$	0.946	0.328	0.808	0.328
$\tau = 1.00$	0.943	0.368	0.809	0.368
$\tau = 2.00$	0.937	0.451	0.815	0.451

Notes: Monte Carlo averages of $\hat{\rho}_C$, $\hat{\rho}_F$, $\hat{\rho}_S$, and $\hat{\rho}_{\min}$ as the out-of-dictionary component $\Gamma_R = \tau BB'/n$ grows. Smaller values indicate a closer fit between the empirical dependence operator and the corresponding covariance geometry.

As τ grows from 0 to 2, $\hat{\rho}_{\min}$ rises monotonically from 0.274 to 0.441, confirming that the out-of-dictionary component makes the operator progressively harder to approximate by any single geometry; $\hat{\rho}_F = \hat{\rho}_{\min}$ throughout because the mixed DGP’s dominant factor component (from the large-norm Σ_F) makes the factor projection the binding constraint at every τ .

E.8 Misspecified Dependence Operators

The results above assume the empirical dependence operator preserves the relevant dependence information. We study operator misspecification by supplying the projection step with deliberately incomplete dependence operators. The purpose is not to show that the

procedure recovers structure absent from its input, but to confirm that the profile and residual diagnostics faithfully describe the geometry encoded in whichever operator is supplied, consistent with the dependence-sufficiency principle of Section 4.1.

Table E.4: Dependence Profiles under Operator Misspecification

True DGP	Operator Used	$\hat{\omega}_C$	$\hat{\omega}_F$	$\hat{\omega}_S$	$\hat{\rho}_{\min}$
Sparse	Full covariance	0.278	0.314	0.409	0.838
Sparse	Diagonal only	0.333	0.333	0.333	0.000
Cluster	Full covariance	0.454	0.199	0.347	0.654
Cluster	Cluster support removed	0.216	0.403	0.381	0.827

Notes: “True DGP” is the dependence mechanism used to generate the data; “Operator Used” is the empirical operator supplied to the projection step. $\hat{\omega}_C, \hat{\omega}_F, \hat{\omega}_S$ are average estimated similarity scores and $\hat{\rho}_{\min}$ the average minimum projection residual. Misspecified operators deliberately discard part of the relevant dependence information.

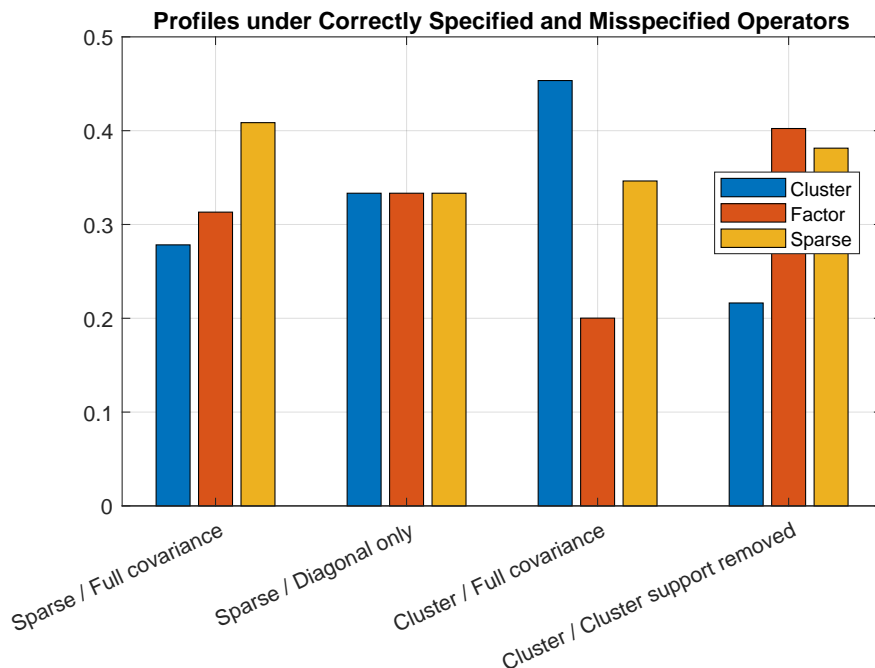


Figure E.2: Dependence Profiles under Correctly Specified and Misspecified Operators

When a sparse-network DGP is summarized by a diagonal-only operator, the sparse score loses its identifying information; when a cluster-dependent DGP is summarized by an operator with cluster-support entries removed, the cluster score is attenuated and $\hat{\rho}_{\min}$ rises. Neither result is a failure of the projection step: the procedure correctly learns the geometry encoded in the operator it is given, not latent dependence mechanisms removed before the projection stage.

E.9 Procedure Recommendation: Variance Estimators and Detailed Results

Section 8.3 of the main paper reports the headline oracle-equivalence result across all three baseline geometries. This subsection gives the variance-estimator formulas behind that result and a more granular two-DGP breakdown that decomposes the finding by the procedure confidence index $\hat{\kappa}$.

For each of the pure Cluster and pure Factor DGPs, β is estimated by averaging OLS over $T = 50$ periods, $\bar{\beta} = T^{-1} \sum_t \hat{\beta}_t$, and $H_0 : \beta_2 = 1$ is tested at the 5% level using one of three variance estimators:

$$\begin{aligned} \hat{V}_C &= \frac{G}{G-1} \cdot \frac{n-1}{n-k} (X'X)^{-1} \left(\sum_{g=1}^G \mathbf{s}_g \mathbf{s}_g' \right) (X'X)^{-1} / T^2, & \mathbf{s}_g &= X_g' \sum_{t=1}^T \hat{u}_{gt}, \\ \hat{V}_F &= (X'X)^{-1} X' \hat{P}_F(\hat{\Gamma}) X (X'X)^{-1} / T, & \hat{\Gamma} &= T^{-1} \sum_t \hat{u}_t \hat{u}_t', \\ \hat{V}_W &= (X'X)^{-1} X' \text{diag}(\bar{u}^2) X (X'X)^{-1} / T, & \bar{u}_i &= T^{-1} \sum_t \hat{u}_{it}. \end{aligned}$$

The profile-guided choice selects \hat{V}_C when $\hat{d} = \arg \max_d \hat{\omega}_d = C$ and \hat{V}_F when $\hat{d} = F$, from the same replication used to compute the profile.

The mean confidence index reveals why both DGPs achieve the near-perfect classification rate reported in the main text despite different finite-sample behavior. For the *factor DGP*, $\hat{\kappa} = 0.489$: the factor projection has low absolute residual *and* a clearly dominant score, so the recommendation is highly reliable. For the *cluster DGP*, $\hat{\kappa} = 0.037$: the cluster projection captures all within-cluster entries in population, but in finite samples the averaged operator's cross-cluster sampling noise inflates $\hat{\rho}_{\min}$, holding $\hat{\kappa}$ down despite correct classification. The population index κ_0 in Table 1 confirms both designs are highly separable in population, so the finite-sample gap is sampling variability in $\hat{\Gamma}$, not a defect in the classifier. Consistent with this, \hat{V}^* achieves near-nominal size under the cluster DGP despite the low $\hat{\kappa}$, and the profile-weighted combination \hat{V}^{avg} performs similarly to \hat{V}^* throughout, confirming that the profile's information is sufficient on its own, without requiring a hard classification step.

A factor-SE finite-sample distortion and its fix. The factor DGP row shows \hat{V}_F rejecting at a rate well above the 5% nominal level even when Factor is correctly recommended. The cause is a structural identity, not ordinary sampling noise: because $\hat{\Gamma} = T^{-1} \sum_t \hat{u}_t \hat{u}_t'$ is built from per-period OLS residuals on the same fixed X , the normal equations give $X' \hat{u}_t = 0$ exactly for every t , so $X' \hat{\Gamma} X = 0$ exactly in every sample. The nonzero $X' \hat{P}_F(\hat{\Gamma}) X$ that survives in \hat{V}_F is therefore driven by the alternating projection's truncation error relative to

Table E.5: Profile-Guided Procedure Recommendation: Detailed Breakdown

DGP	Profile	Mean $\hat{\kappa}$	$P(\hat{d} = d^*)$	Cluster SE	Factor SE	White SE	\hat{V}^* (rec.)	\hat{V}^{avg} (wtd.)
Cluster	$\hat{\omega}_C$ dom.	0.037	1.000	0.069	0.065	0.785	0.069	0.139
Factor	$\hat{\omega}_F$ dom.	0.435	1.000	0.078	0.300	0.787	0.300	0.320

Notes: $B = 1,000$ replications, $n = 250$, $T = 50$. Mean $\hat{\kappa}$: average procedure confidence index $\hat{\kappa} = (1 - \hat{\rho}_{\min})\hat{\Delta}_{\omega}$. \hat{V}^* (rec.): rejection rate using the profile-recommended estimator. \hat{V}^{avg} (wtd.): rejection rate using the profile-weighted combination $\hat{V}^{\text{avg}} = \sum_d \hat{\omega}_d \hat{V}_d$ (Section 7.5).

$\widehat{\Gamma}$ rather than genuine factor signal, and recovers only 10–15% of the true sandwich variance in this design. Time-demeaning the *outcome* within each cross-sectional unit before forming the operator, $\widetilde{Y} = Y - \bar{y}\mathbf{1}'_T$ with $\bar{y}_i = T^{-1}\sum_t y_{it}$, avoids the degeneracy because $x'_i\beta$ is constant across t and is removed exactly without ever residualizing on X . The corrected estimator $\widehat{V}_F^{\text{corr}}$ (`vcov_factor_LD_corrected.m`) recovers approximately 99% of the true sandwich variance in the same design and is used as the Factor SE throughout the headline oracle-equivalence table in the main paper. This diagnosis is general: it applies to any panel setting in which a factor-structured plug-in covariance is built from residuals that have already been projected against the same regressors used in the sandwich.

E.10 Oracle Tracking along a Continuous Dominance Sweep

The two pure-DGP rows above show fixed procedures can be badly miscalibrated under the “wrong” dependence structure, which raises a natural question: why learn the geometry at all, rather than adopt one procedure—two-way clustering, say, or a fully heteroskedasticity-and-autocorrelation-robust sandwich—that is valid under a wide range of dependence patterns? Procedures built for broad robustness are not free: they sacrifice power or stability precisely where a more specific procedure would have been valid *and* more informative, and a procedure robust against one geometry need not behave well under another even when both are well understood individually. The profile-guided approach lets the data reveal which geometry is operative, at no asymptotic cost relative to knowing the answer in advance (Theorem 7). We verify this directly along a continuous Cluster–Factor dominance sweep,

$$\Sigma(\alpha) = \alpha^2\Sigma_C^{\text{pure}} + (1 - \alpha)^2\Sigma_F^{\text{pure}} + \sigma_\varepsilon^2 I_n, \quad \alpha \in [0, 1],$$

the same path underlying Figure 1, reporting rejection rates for the fixed Cluster and Factor SEs, the profile-guided $\widehat{V}^\star = \widehat{V}_{\widehat{d}}$, and the infeasible oracle \widehat{V}_{d^\star} at $d^\star = \arg \max_d \omega_d(\alpha)$.

Cluster SE remains close to nominal across the sweep, but Factor SE is badly oversized exactly where Factor dependence dominates ($\alpha \leq 0.625$): 29.2% rejection at $\alpha = 0$, falling to 8.1% at $\alpha = 0.625$ before returning toward nominal as Cluster takes over—the same finite-sample distortion diagnosed above, now traced across a continuum rather than two points. Because classification is essentially perfect throughout ($P(\widehat{d} = d^\star) \geq 0.929$, equal to 1.000 at all but one point), \widehat{V}^\star and \widehat{V}_{d^\star} are within 0.002 of each other at every α , including the one point with imperfect classification—the profile-guided procedure inherits whatever distortion its selected base estimator carries, but never does meaningfully worse than the oracle using that same estimator, exactly the content of Theorem 7.

Repeating the sweep with $\widehat{V}_F^{\text{corr}}$ in place of \widehat{V}_F (Table E.7) shows both fixed procedures

Table E.6: Oracle-Tracking Diagnostic along the Cluster-Factor Dominance Sweep

α	Pop. dominant	$\omega_C - \omega_F$	$P(\hat{d} = d^*)$	Cluster SE	Factor SE	\hat{V}^* (profile)	\hat{V}_{d^*} (oracle)
0.000	Factor	-0.666	1.000	0.072	0.292	0.292	0.292
0.125	Factor	-0.664	1.000	0.061	0.239	0.239	0.239
0.250	Factor	-0.661	1.000	0.066	0.205	0.205	0.205
0.375	Factor	-0.648	1.000	0.055	0.142	0.142	0.142
0.500	Factor	-0.593	1.000	0.074	0.113	0.113	0.113
0.625	Factor	-0.337	1.000	0.063	0.081	0.081	0.081
0.750	Cluster	0.226	0.929	0.061	0.071	0.063	0.061
0.875	Cluster	0.431	1.000	0.066	0.070	0.066	0.066
1.000	Cluster	0.454	1.000	0.069	0.068	0.069	0.069

Notes: $B = 1,000$, $n = 250$, $T = 50$, nominal level 5%. Cluster SE and Factor SE use the FIXED estimator at every α , regardless of which geometry dominates; \hat{V}^* estimates \hat{d} from the same replication; \hat{V}_{d^*} uses the true dominant geometry, infeasible in practice.

Table E.7: Oracle-Tracking Diagnostic, Bias-Corrected Factor SE (Robustness Check)

α	Pop. dominant	$\omega_C - \omega_F$	$P(\hat{d} = d^*)$	Cluster SE	Factor SE (corr.)	\hat{V}^* (profile)	\hat{V}_{d^*} (oracle)
0.000	Factor	-0.666	1.000	0.065	0.054	0.054	0.054
0.125	Factor	-0.664	1.000	0.056	0.052	0.052	0.052
0.250	Factor	-0.661	1.000	0.076	0.058	0.058	0.058
0.375	Factor	-0.648	1.000	0.072	0.069	0.069	0.069
0.500	Factor	-0.593	1.000	0.064	0.056	0.056	0.056
0.625	Factor	-0.337	1.000	0.067	0.048	0.048	0.048
0.750	Cluster	0.226	0.924	0.062	0.049	0.061	0.062
0.875	Cluster	0.431	1.000	0.064	0.054	0.064	0.064
1.000	Cluster	0.454	1.000	0.060	0.042	0.060	0.060

Notes: Identical design to Table E.6, with \hat{V}_F replaced by \hat{V}_F^{corr} (`vcov_factor_LD_corrected.m`).

reasonably well sized against each other’s misspecification throughout (rejection rates between 4.2% and 7.6%), with the profile-guided estimator continuing to track the oracle exactly—confirming that the oracle-adaptivity result is not an artifact of the uncorrected estimator’s distortion. Figure 3 in the main paper plots the original (uncorrected) sweep; the profile-guided and oracle curves are visually indistinguishable throughout, and the two fixed-procedure curves cross only once, near $\alpha \approx 0.7$, inside the region where the population margin $\omega_C - \omega_F$ is still modest—exactly where a researcher committing to one procedure in advance would be most likely to guess wrong.

A Empirical Details

The empirical illustration uses the Fama–French 49 industry portfolios and the Fama–French factors. The main paper describes the construction of the residual covariance and correlation operators. The replication package documents the complete sector mapping, data downloads, transformations, and software used to generate the empirical tables.